Geological Features and Evolution of Yardangs in the Qaidam Basin, Tibetan Plateau (NW China): A Terrestrial Analogue for Mars

Jiang Wang[1], Long Xiao[1,2]*, Dennis Reiss[3], Harald Hiesinger[3], Jun Huang[1], Yi Xu[2], Jiannan Zhao[1], Zhiyong Xiao[1,2] and Goro Komatsu[4]

[1] State Key Laboratory of Geological Processes and Mineral Resources, Planetary Science Institute, School of Earth Sciences, China University of Geosciences, Wuhan, China.

[2] Space Science Institute, Lunar and Planetary Science Laboratory, Macau University of Science and Technology, Taipa, Macau, China.

[3] Institut für Planetologie, Westfälische Wilhelms-Universität, Münster, Germany.

[4] International Research School of Planetary Sciences, Università d'Annunzio, Pescara, Italy.

* Corresponding author: Long Xiao (longxiao@cug.edu.cn)

School of Earth Sciences, China University of Geosciences, Wuhan 430074, China.

Key Points:

- We conduct a comprehensive study of geomorphology and evolution processes of yardangs in the Qaidam Basin and their analogues on Mars.
- These yardangs have similar morphologic and geometric characteristics, and experienced a multi-stage evolution.
- The evolution processes may have been interrupted at some stages due to differences in rocks properties and/or the changes of environment.

This article has been accepted for publication and undergone full peer review but has not been through the copyediting, typesetting, pagination and proofreading process which may lead to differences between this version and the Version of Record. Please cite this article as doi: 10.1029/2018JE005719

Abstract

Wind-eroded ridges known as yardangs are common in most arid desert regions on Earth, as well as on other planets, notably in the Medusae Fossae Formation (MFF) and Gale Crater on Mars. However, the formation and evolution of these various yardangs are not well understood, which, therefore, requires further studies by more terrestrial analogues. Here we report a detailed investigation of the terrestrial yardang fields in the Qaidam Basin, northeastern Tibetan Plateau, China. Most of them are distributed in the northwestern and central eastern parts, with dominant orientations northwest to north-northeast and approximately west to east, respectively. Based on their morphologies and distributions, yardangs within the Qaidam Basin have been classified into 11 different types out of four main groups.Wind is the dominant driver of yardangs erosion, but water, salt, and mass wasting may also have played important roles in their formation and modification. A four-step evolution model, including embryonic, adolescent, mature, and receding stages, is proposed to reveal their formation and evolution in the basin. Meanwhile, yardangs in the Medusae Fossae Formation and Gale Crater on Mars have morphologic and geometric characteristics which show striking similarities to those in the Qaidam Basin. The facts that some yardang fields in MFF on Mars also show overlapping relationships suggest that they possibly have experienced a multi-stage evolution, during which the evolution processes may have been interrupted at some stages due to differences in the competence of rocks and/or the changes of environment.

Key words: yardang, Qaidam Basin, Medusae Fossae Formation, Gale Crater, analogue

Plain Language Summary

The Qaidam Basin is the largest yardang field in China. In this study, we investigate the distributions, morphological types, and sizes of these yardangs. We attempt to explore their origins and explain their evolution processes. Based on their morphologies and distributions, we have identified 11 different types of yardang and sort them into four main groups. We find both their spatial distribution and orientation are controlled by local topography and prevailing wind direction. Their main orientations are northwest to north-northeast in the northwestern basin, while approximately West to East in the central eastern basin. Yardangs in the Qaidam Basin are mainly eroded by wind. We propose a four-step evolution model to explain their formation processes. Similar yardangs on Mars are also observed, such as those within the Medusae Fossae Formation and Gale Crater. We find that yardangs on Mars show morphologic and geometric characteristics similar to those in the Qaidam Basin, indicating they may have experienced similar evolution processes.

1 Introduction

"Yardang" is a geological term that was introduced by Hedin (1903) when he travelled the Lop Nur, northwestern China to define the streamlined, wind-carved ridges that had been developed within lacustrine deposits. This term has now been extended to define wind-carved ridge-like features in general, whether highly streamlined or not (Halimov & Fezer, 1989; Laity, 2011). Typical yardangs occur mostly in large fields, and they are observed in arid to hyper-arid regions where havesparse vegetation and annual precipitation less than 50 mm (Niu et al., 2011). The majority of deserts on Earth, including Central Asia, Southern Iran, Northern Saudi Arabia, Bahrain, Namibia, Egypt, southern California, Central Sahara, the high Andes of South America, and the coastal Peru and Chile (cf. Goudie, 2007; McCauley et al., 1977a), all host yardangs. They have also been identified on other planets, i.e. Venus (Greeley et al., 1992), Titan (Paillou & Radebaugh, 2013), and especially on Mars (Carr, 2007), where yardangs typically occur in equatorial regions, including the Medusae Fossae Formation (MFF), Ares Vallis, Sacra Sulci, Candor Chasma, Iapygia and some paleolake basins within impact craters (Day & Kocurek, 2016; Desai & Murty, 2016; Greeley & Iversen, 1987; Kite et al., 2013; Tanaka et al., 2014; Ward, 1979).

Most of yardang fields in China occur in the Qaidam Basin, along the middle and lower Shule River, and in the Xinjiang Province (Yang, 2009). The Qaidam Basin hosts the largest yardang field in China, covering an area of about 3.88×10^4 km^2 (Kapp et al., 2011; Li et al., 2016), nearly one-third of the basin. Only a few studies on these yardangs have been carried out due to their remote location and a challenging environment. Based on fieldwork, Fan (1962) described the morphology of yardangs in Lenghu area, northwest of the basin, and classified them into three different types: "pyramid", "earth hummock", and "long-ridge". With the aid of stereo images acquired by the space shuttle Columbia and field inspections, Halimov and Fezer (1989) further divided the yardangs between Daqaidam and Lenghu into eight types, comprising "mesa", "saw-toothed crest", "cone", "pyramid", "hogback", "whaleback", and "low, streamlined whaleback" yardangs. Later, a few research groups have investigated the yardangs in other restricted areas within the Qaidam Basin. Hu (1990) divided the yardangs in Qarhan, center of the Qaidam Basin, roughly into young, mature and decline stages without specific descriptions, and Li et al. (2011; 2013) studied their morphologies, sediments, and wind regimes. Wei (2013) focused on the hogback yardangs in Kaitemilike, southwest of the basin, and described their possible formation processes. Based on the classification from Halimov & Fezer (1989), Li et al. (2016) mapped the "mesa", "long-ridge", "saw-toothed crest", and "whaleback" yardangs in the western Qaidam Basin. Hu et al. (2017) classified the yardangs into four types with multi-source remote sensing data based on their length/width ratios. However, previous researches covered only some parts of the basin, and the insufficient data have constrained our understanding about the comprehensive characteristics, formation and evolution of the yardangs in the Qaidam Basin.

Many formation and evolution models of the yardangs on Earth have been proposed. Halimov and Fezer (1989) suggested that the troughs in-between yardangs were carved by occasional fluvial activities during their early stage, and then, enlarged by wind. The

yardangs are shortened and lowered due to continual erosions and collapses. Embabi (1999) proposed a four-stage (juvenile, mature, advanced, end stages) evolution model for the long-ridge yardangs developed in the Holocene playa sediments overlying bedrock in the western desert of Egypt, and Brookes (2001) applied this model to yardangs in the Libyan Desert which are developed exclusively in bedrock. Both of their models described the evolution progresses from long-ridge yardangs with narrow troughs (juvenile stage) to broad troughs (mature stage), then shorten in length (advanced stage), enlarging in spacing (end stage), and finally ending with planation. Dong et al. (2012) proposed a similar four-stage (embryonic, adolescent, mature, and receding) development for the long-ridge yardangs in the Kumtagh Desert, NW China. The difference is that the receding form of yardangs in the Kumtagh Desert are still with long-ridge shapes with narrow tops and broad troughs, which are equal to the mature stage in Embabi's model. However, the development of yardangs in the Qaidam Basin seems to be much more complex than those above mentioned judging criteria (types, size, and morphologies). Therefore, further studies are necessary to account for their formation and evolution.

In order to fully understand the formation and evolution of martian yardangs, distinct yardangs in the Qaidam Basin can also shed light on the geological history of Mars (Xiao et al., 2017; Anglés & Li, 2017; Li et al., 2018). Preliminary observations show that the yardang fields in the MFF on Mars are abundant, highly complex, and similar to those occurring within the Qaidam Basin. Previous investigations have reported some yardangs in the MFF (e.g. Kerber & Head, 2010; Mandt et al., 2008, 2009; Zimbelman & Griffin, 2010), and provided "v-shaped depressions origin" (Mandt et al., 2009; Mandt et al., 2008) and "lava casts" (Kerber and Head, 2010) models to describe their formation and evolution. However, the limited coverage of high-resolution images has constrained the size of research areas, and more small-sized yardangs of different types have been reported recently (Day & Kocurek, 2016; Desai & Murty, 2016; Li et al., 2018; Zaki, 2016) thanks to the increasing coverage of high-resolution images obtained by the Mars Reconnaissance Orbiter (MRO). Previous models account for only a few yardangs formation, and the evolution among different yardang types remain uncertain and demand further studies, which means that more analogue studies are required to better understanding of their formation history and relevant climate environment of this region. The Curiosity rover (Mars Science Laboratory, MSL) is continuously studying yardangs within Gale Crater (centered at 5.4°S, 137.7°E). Their morphologies and distributions have been described (Fairén et al., 2014; Le Deit et al., 2011, 2013), but studies about the detailed evolution processes are still lacking. Correlations and comparative studies of yardangs in the MFF and Gale Crater would be helpful for our better understanding of yardangs formation and evolution on Mars (Dapremont et al., 2014; Mandt et al., 2008; Milliken et al., 2010; Thomson et al., 2008, 2011; Zimbelman & Scheidt, 2012).

In this paper, we provide a completed survey of all the yardangs within the Qaidam Basin, integrating high-resolution images taken by a drone (Unmanned Aerial Vehicle, UAV) and satellites, and fieldwork during the past four years.The detailed geological features, geometric parameters, possible evolution history, and controlling factors in the development of the yardangs are described and discussed. Similar-shaped yardangs in the MFF and Gale

Crater on Mars are compared, with their counterparts in the Qaidam Basin, yielding a new model to describe the formation and evolution of yardangs in the MFF and Gale Crater.

2 Geological setting and climate

2.1 Geological setting of the Qaidam Basin

The Qaidam Basin is located between 90°16' E – 99°16' E and 35°00' N – 39°20' N in northwestern China (Figure 1). As the largest intermontane sedimentary basin along the northeastern Tibetan Plateau, it covers about 120, 000 km^2 (~700 km long and up to ~300 km wide) in area, with an average elevation of ~2800 m, making it one of the highest deserts in the world (Rohrmann et al., 2013). Topographically, it is bounded by the Altyn Tagh Range to the northwest, the East Kunlun-Qiman Tagh orogenic belt to the south-southwest, and the Qilian orogenic belt to the north-northeast (Yin et al., 2008), showing as a triangular shape in plane view (Figure 1a).

The Qaidam is a tectonically controlled sedimentary basin (Yin et al., 2002). Since the middle to late Miocene, it has been compressed and actively shortened in the NE – SW direction due to the ongoing convergence between India and Eurasia plates (Tapponnier et al., 2001; Wu et al., 2014; Zhang et al., 2004), and also NW – SE and NNW – SSE trending folds are developed in the sediments of western basin (Wang et al., 2012a; Zhang et al., 2013). These folds separated the basin into several sub-basins sometimes hosting lakes (Fang et al., 2007; Han et al., 2014; Wang et al., 2006; Wang et al., 2012b).

The basement outcrops emerge along the edge of the Qaidam Basin, consisting of Precambrian – Silurian metamorphic rocks (e.g. Huang et al., 1996). The overlain stratum within the basin are Devonian – Cenozoic sediments that were originated from weathering and denudation of the surrounding mountains (e.g. Yang et al., 2001; Yin et al., 2007, 2008). The total thickness of Cenozoic sediments within the basin can reach up to about12,000 m (Fang et al., 2007; Xia et al., 2001). In the northwestern part, the surface layer of the sub-basins is Pleistocene strata, consisting of cyclic clays, mudstones, evaporites (e.g. halite, gypsum) (Li et al., 2010; Zhang et al., 2012), while most of the outcropped folded structures are Tertiary strata that is mainly made by mudstones, siltstones, and sandstones, with interbedded sulfate (e.g. gypsum) layers. Holocene deposits, including aeolian (e.g. sand dunes), seasonal fluvial, and modern saline lake sediments, are distributed on the north alluvial-diluvial clinoplains of the East Kunlun-Qiman Tagh Mountains (Li et al., 2016) or interspersed in the low-lying areas within the basin (Figure 1).

2.2 Climate in the Qaidam Basin

The Qaidam Basin is mainly influenced by the westerlies (Figure 1a). Due to the shielding effect of the Tibetan Plateau and surrounding high mountain ranges, little moisture can reach in this Eurasian hinterland basin after a long trip. The main moisture source is carried by the East Asian Monsoons, which can extend to the southeastern basin after crossing the Hengduan Mountains. Most of rainfalls come from the convergence zone of these two flows, but both of them are very little (Wu et al., 1985; Wu, 2009). Thus, their

influences decline from east to west throughout the basin. The annual precipitations are ~150 mm – ~200 mm, ~40 mm – ~50 mm and <50 mm – <20 mm in the southeastern, central and northwestern basin, respectively. While their annual evaporations can be as high as ~2000 – 3600 mm (Wu, 2009; Zhang & Liu, 1985), enabling it to be one of the driest regions on Earth (Rohrmann et al., 2013; Xiao et al., 2017).

The prevailing wind direction in the western basin is NW – SE, and becomes nearly W – E in the eastern part. Except for some closed terrains (e.g. Daqaidam, Delingha), the average monthly wind velocity is > 3 m/s, in the western Laomang'ai area is ~5 m/s, while the maximum historical wind velocity is 40 m/s (Ren, 1996; Rohrmann et al., 2013; Wei, 2013). Annual fresh gale conditions (wind velocity $\geqslant$ 17 m/s) last from 57 to 105 days, with an average of 84.2 days per year. Most of the gale days (about 50% – 70%) occur from March to June (Wu et al., 1985; Wu, 2009).

During the past 32 years (1980 ~ 2011), climate data collected from the meteorological station (Mangya, Dalangtan playa) show that the temperature ranges from < -25 °C (January) to > 30 °C (July), with an annual mean temperature of 3.5 °C (Kong et al., 2018). The annual average air pressure recorded was 709 mbar (Kong, 2013; Kong et al., 2018), about two third of the standard atmospheric pressure.

2.3 Geological settings of the Medusae Fossae Formation and Gale Crater

The MFF is a discontinuous geological unit of soft, easily eroded deposit that extends along the dichotomy boundary in the equator region of Mars from approximately 130° E to 240° E and 15° S to15° N, between the Tharsis and Elysium volcanic provinces (Scott & Tanaka, 1986, Figure 2), covering an area about 2.1×10^6 km^2 with a total volume of ~1.4×10^6 km^3 at present (Bradley, 2002). The main parts include Aeolis Planum, Zephyria Planum, Lucus Planum, Medusae Fossae, Eumenides Dorsum, Amazonis Mensae, Gordii Dorsum, and Gigas Fossae (Kerber et al., 2011; Kerber & Head, 2012, Figure 2). Their surfaces have been extensively reworked by aeolian processes.

Gale Crater is adjacent to the western MFF region, with ~155 km in diameter. It is dominated by a 5.5 km high central mound, named Aeolis Mons, interpreted to a sedimentary sequence (Grotzinger et al., 2014; Milliken et al., 2010; Stack et al., 2016), whose maximum elevation is similar to that of the southern crater rim but is higher than the northern degraded crater rim. Gale is proposed to have hosted a paleolake around 3.5 Gyr ago and formed thick lacustrine sediments (Hurowitz et al., 2017). Thomson et al. (2011) has divided this sedimentary sequence into two parts: a lower member (LM) and an upper member (UM). The lower member is characterized by horizontal to sub-horizontal stratum, while layers in the upper member are much thinner with higher-angle bounding surfaces.

2.4 Current climate of Mars

The current surface average temperature of Mars is about -123 °C to -33 °C (Kieffer et al., 1977), and the daily highest temperature can be reach to 27 °C at some local areas of the mid southern latitude in summer season (Carr, 2007). Compared with the terrestrial

atmosphere, the current martian atmosphere is extremely tenuous, with an average surface atmosphere pressure about 0.5 – 1%, comprising mostly of carbon dioxide (about 95%) with a small amount of nitrogen and argon (Read & Lewis, 2004). The surface wind velocities are variable among separate areas. For example, the wind velocities are usually about 20 m/s to 30 m/s at the Viking lading site, and the highest wind velocity can reach 150 m/s (Chamberlain et al., 1976). While wind velocities obtained from the Rover Environmental Monitoring Station (REMS) onboard MSL range from 0 to 20 m/s, and most of them are 2 m/s to 6 m/s (Viúdez-Moreiras et al., 2017).

3 Data and methods

Our study of the Qaidam Basin yardangs is based on recent multi-year field investigations combined with an analysis of satellite images from Google Earth (https://earth.google.com/). In addition, we used high-resolution (centimeters scale, Reshetyuk & Mårtensson, 2016) air images obtained with a drone (DJI Phantom 4). Digital terrain models (DTMs) were processed from these airborne images using the Agisoft photoscan software (http://www.agisoft.com/). The geometric parameters of the yardangs were measured with ArcGIS using Google Earth images and the profiles were derived from DTMs. We carried out detailed field investigations for ground-truth and field measurements. During the past four-years fieldwork, we examined on-site properties of the yardangs that we measured in the images previously. Taking the regional morphological differences of yardang fields into consideration, the method of classification suggested by Halimov and Fezer (1989) and Li et al. (2016) has been adopted in our study. All of the recognizable yardangs were mapped and shown in Figure 1a.

For the study of yardangs on Mars, we primarily used Context Camera (CTX, Malin et al., 2007) data (6 m/pixel) since they are provided with a wide coverage (over 99%) of the Mars. Detailed observations were conducted with the High Resolution Imaging Science Experiment (HiRISE, McEwen et al., 2007) data (up to 25 cm/pixel). We also produced and analyzed CTX DTMs and HRSC (High Resolution Stereo Camera) DTMs in addition to the MOLA (Mars Orbiter Laser Altimeter) DTMs for high-resolution topographic analysis. CTX DTMs were processed by the MarsSI (emars.univ-lyon1.fr) application with the Ames Stereo Pipeline (ASP, Moratto et al., 2010). The HRSC DTMs are downloaded from the Mars Orbital Data Explorer (MODE, http://ode.rsl.wustl.edu/mars/).

4 Yardangs in the Qaidam Basin

4.1 Classification

In this study, we classify the yardangs in the Qaidam Basin into 11 different types and sort them into 4 groups (Table 1) mostly on the basis of their morphologies and distributions. Taking into account of their morphological complexities and distributions in field, our priority researches are the morphologic (Table 1) and geometric (Table 2) characteristics of representative yardangs in the Qaidam Basin.

4.1.1 Mesa group yardangs

The mesa group (M group) yardangs include two different types, irregular (M-I type) and elongated mesa (M-E type) yardangs, both of them are elevated steep-sided and flat-topped hills (Figure 3 and 4). The M-I type yardangs develop in piedmont layered alluvial-diluvial clinoplains (Figure 3a, 3b, and 3c). They are large in size (up to ~60 km long and 1 km wide), and exhibit various shapes, ranging from irregular (Figure 3b and 3c) to dendritic (Figure 3a). Aeolian sediments and slope debris accumulate at the foot of these mesas (Figure 3d). Some gravel-enriched polygons (~1 m in diameter) are observed on their surface, and gullies occur at their rim (Figure 3d). Some M-I type yardangs are developed at the western margin of the playa with obvious light wind streaks (salt) (Figure 13c).

The elongated mesa (M-E type) yardangs are usually in rhombus shape with a flat top on the head, surrounding cliffs, and a relative gentle slope at the leeward end. They are more streamlined than the M-I type yardangs. Generally, the leeward surfaces are covered by salt crusts exhibiting polygons, while the windward surfaces expose the original horizontal lacustrine sediments (Figure 4d), sometimes with moats surrounding them (Figure 4b). Overall, these M-E type yardangs are usually arranged in lines with one direction or two directions (Figure 4a and 13e).

4.1.2 Long-ridge group yardangs

Morphologically, the long-ridge group (L group) yardangs contain three different types, i.e., broad-top long-ridge (L-B type, Figure 5a), narrow-top long-ridge (L-N type, Figure 6a) and rough-top long-ridge (L-R type, Figure 6c) yardangs.

The L-B type yardangs are usually parallel to each other and extend continuously for nearly 4 km at maximum. They have a broad top, two gentle convex flanks and narrow troughs in-between them (Figure 5a). On the upwind side, the broad tops are eroded into small ridges with tapered heads (Figure 5b), while their downwind areas are still unaltered. The flanks of the new heads become much steeper. In some places, remnant cap layers occur on the top surface (Figure 5b). Large polygons developed both on the surface of the yardangs and in the troughs (Figure 5c).

The L-N type yardangs are also orientated parallel to each other but are less continuous. They have narrow tops, steep flanks and wide troughs in-between them (Figure 6a). They are much shorter and narrower than the L-B type yardangs and even consist of only a wall (~1 m thick) with nearly vertical flanks. Mass wasting derived slope debris covers the lower parts of the yardangs. Colorful multilayered lacustrine sediments have been observed in the field, with remnant cap layers on their top surfaces, but no obvious salt crusts are found on the L-N type yardangs (Figure 6b).

The L-R type yardangs are ambiguous in morphology, but still can be recognized from the parallel troughs and extensively broken tops (Figure 6c). Original broad tops are eroded into fragments or small ridges with faceted surfaces, which seem to be rather rough in satellite images.

4.1.3 Saw-toothed group yardangs

The saw-toothed (S-T type), pyramid (S-P type), remnant cone (S-R type) yardangs are usually coexisting in the Qaidam Basin, so we consider them as one group, and here we describe each representative type individually. The S-T type yardangs show zigzag-like morphologies (Figure 7a and 7b). Layers exposed at their windward sides are eroded into small ridges (Figure 7c). Most of their downwind sides are still unaltered, while some of them with saw-teeth separated from their downwind sides exhibit as W-B or W-H type yardangs (Figure 7a). In the yardang fields, salt crusts with small polygons on the top surfaces and gypsum-enriched floors are observed (Figure 7c). The S-P type yardangs look much more angular, exhibiting as large pedestals and spire tops (Figure 7d) with no distinct coverings. The S-R type yardangs appears to be truncated cones. They usually have rounded shapes (Figure 7e) or with small flat tops.

4.1.4 Whaleback group yardangs

The whaleback (W-B type), hogback (W-H type), and low, streamlined whaleback (W-L type) yardangs often occur in groups mixed together in the fields, thus makes it difficult to separate individual types from each other. Considering their similar morphologies, we treat them as one group.

The W-B type yardangs are archetypical yardang forms with blunt heads, convex flanks, and tapered tails. Viewed from the side, they show whaleback morphologies (Figure 8a). They commonly have a thick (~50 cm), hard, salt crust covering horizontally bedded lacustrine sediments (Figure 8b). Some small gullies carved by rainfalls on their flanks are obvious in these yardang fields.

The W-H type yardangs have steep windward slopes (mostly >60°) and tapered tails (Figure 8c, 8d, and 8e), and some have undercut windward heads (Figure 19a). They are similar in morphology to the W-B type yardangs but are much larger in size and relatively less streamlined. They usually have sharp crestlines on their backs (Figure 8c). Some of their windward faces show evidence of collapses (Figure 8c). In addition, their flanks are distinct from the W-B type yardangs. Some small W-H type yardangs exhibit slightly convex flanks, while some larger W-H type yardangs are characterized by convex flanks at the lower parts and concave flanks on their upper parts (Figure 8c and 8d). Their lower parts are usually covered by salt crusts but their upper parts consist of exposed bedrocks (Figure 8d). In contrast, the W-L type yardangs are relatively aerodynamically shaped and display perfect "teardrop"-like morphologies in plane view (Figure 8f and 8g). They are smaller in size than the W-B type and W-H type yardangs, and usually have much larger spacing (Figure 8f). Their surfaces are covered by polygonal fractured salt crusts (Figure 8g).

4.2 Distribution

As previously reported and found in this study, yardangs in the Qaidam Basin are mainly distributed in the northwestern and central eastern parts (Figure1). Generally, in the northwestern basin, their periphery is surrounded by modern piedmont alluvial-diluvial fans

in the northern and northeastern parts, and sand fields in the southwestern part. While in the southern of the northwestern part, they are bounded by playas, active saline lakes and rivers (Halimov & Fezer, 1989; Li et al., 2016). In the central eastern part, yardangs are mainly bounded by active rivers and alluvial-diluvial fans (Figure 1).

The M-I type yardangs are mainly distributed in areas with piedmont alluvial-diluvial paleo-clinoplains, and occur sporadically inside the western basin. The typical area is between Mahai and the Xiaoqaidam Lake, and the southern margin of the Altyn Tagh Mountains. The M-E type yardangs occur mainly in the bidirectional winds region, downwind of the L group yardangs. The typical area is between Dafengshan and Tulinbao.

The L group yardangs are mainly distributed in the areas surrounding the Qahansilatu playa, Kunteyi playa, and the north area of Nuomuhong. The L-B and L-N type yardangs in the western basin occur mostly in early-middle Pleistocene strata consisting of cyclic clays, mudstone, and evaporites (e.g. gypsum) (Li et al., 2010; Zhang et al., 2012). The L-N type yardangs in the north of Nuomuhong formed on the Holocene flood plain of the Qaidam River. The L-R type yardangs mainly occur between E'boliang and Nanbaxian in Neogene strata comprising mudstone, sandstone, calcareous mudstone, interbedded with siltstone, gypsum, nodular limestone, and bedded rock salt (Zhong et al., 2004).

The S group yardangs are mapped according to the locally most abundant type. They usually develop in folded stratum (Fan, 1962), which have similar dip directions with prevailing winds (Figure 7b). Most of them are located in the southeastern limbs of anticlinal folded structures. They usually occur in Miocene - middle Pleistocene mudstones. The best developed S-P type yardangs are found in the Daxiongshan uplift (E'boliang Yardang Geopark) (Figure 7d).

The W group yardangs are widely spread throughout the basin. They were mapped according to the locally most abundant type. The W-B type yardangs typically occur in the Dalangtan area consisting of Pliocene and early - middle Pleistocene mudstones. The W-H type yardangs mainly develop in early - middle Pleistocene mudstones which are distributed in the large area of the northwestern basin. The W-L type yardangs appear only in small areas in the basin. One representative area is in the north of the East Taijinaier Lake. They occur in Upper Pleistocene strata, which are characterized by evaporites.

4.3 Morphometry

We measured geometric parameters (length, width, spacing, and orientation) and used these parameters to describe different yardang groups (Table 2). The S group and the L-R type yardangs are not included here because of their ambiguity in length and width, but we measured their orientations (Figure 10). Due to the irregular shapes of the M-I type yardangs, we only describe their sizes for reference but have not included them in Table 2.

The M-I type yardangs are present in sinuous shape with length up to ~60 km, and widths up to 1 km, and heights of 10-80 m. The M-E type yardangs are smaller in size. Their lengths range from 18 to 317 m (Figure 11a), with an average value of 167 m. They are 15-

242 m wide (Figure 11b), with an average value of 66 m. The lengths of the L group yardangs vary from 43 to 3903 m (Figure 11a), with an average value of 634 m. Their widths range from 6 m to 219 m (Figure 11b), with an average value of 39 m. The heights of these yardangs can reach to 30 m. The lengths of the W group yardangs range from 5 to 654 m (Figure 11a), and their widths range from 3 to 182 m (Figure 11b). The W-L type yardangs usually have heights of 0.5-4 m, whereas the heights of W-H yardangs can be up to 30 m (Table 2).

These geometric characters resulted from the yardangs' forming mechanisms. Grolier et al. (1980) found that wind streamlined yardang appears to have an aspect ratio value (length/width) of 3:1 or greater, which has been suggested to be can a critical parameter to distinguish yardangs from other hills. In fact, their aspect ratios are associated with the duration for erosion, the strength of wind, and the competence of rock into which they are carved (Laity, 2011). On the basis of fluid mechanics and aerodynamical theoretical calculations, Fox and McDonald (1973) found that the long-ridge yardangs with large aspect ratio values are formed by strong skin-friction drags, whereas yardangs with small aspect ratio values are formed by pressure drags. When the aspect ratio value is about 4:1, the total drag reaches the minimum. Under these conditions, the yardangs have morphologies that are much more streamlined. Wind tunnel experiments also suggest an ideal aspect ratio of 4:1, independent of scale (Ward & Greeley, 1984). However, in the yardang fields, the formation of these ideal-shape yardangs will experience much longer time than their simulants and the actual aspect ratio values vary substantially. For yardangs in the Qaidam Basin, their aspect ratio values vary from 1:1 to 75.4:1. For M-I type yardangs they range from 1:1 to 8.8:1, with an average value of 2.7:1, and most of them have aspect ratio values less than 5:1 (Figure 9a). The L group yardangs have much larger aspect ratio values that range from 2.6:1 to 75.4:1, with an average value of 15.5:1, most of them being greater than 5:1 (Figure 9b). The W group yardangs include aspect ratio values between 1.1:1 and 13:1, with an average value around 3:1 (Figure 9c). The yardangs with aspect ratios between 3:1 and 5:1 show much more streamlined morphology, whereas the long-ridge yardangs are mostly with aspect ratio values greater than 5:1.

The orientation of yardangs is usually controlled by the local dynamical conditions. The long axes of yardangs sculpted by wind are largely subparallel to the direction of the prevailing wind or, the maximum wind velocity, whereas the orientation of yardangs formed or modified by ephemeral water, may be consistent with the flow direction of the water (Hörner, 1932; Krinsley, 1970; Laity, 2011; Xia, 1987). If the yardangs were eroded by both processes, wind and water, then their orientations might exhibit an angle between them (Xia, 1987). The orientations of yardangs and dunes in deserts recored the local prevailing wind directions during their evolutions (Figure 1a). In the Qaidam Basin, northwest winds pass through the topographic lower areas (pathway a, b, and c in Figure 1a) of the Altyn Tagh Ranges into the basin(Halimov & Fezer, 1989), which become more westerly when pass through west to east. This variation is consistent with the trends of the southern East Kunlun mountains (Kapp et al., 2011). The M-E type yardangs developed in the downwind direction of the L group yardangs. Their dominant long axis orientations range from NNW to N

(Figure 13e and 10a), which coincides with the L group yardangs developed in the upwind direction (Figure 13e). The L group yardangs in the northwestern basin are orientated from NNW to N in fan-shaped scattered from the wind pathway in the Altyn Tagh Mountains, whereas the L group yardangs in the north of Nuomuhong are orientated nearly W to E (Figure 1a and 10b). The S-T type yardangs are orientated from NW to N, and the dominant orientation is NNW (Figure 10c). The dominant orientations of the W-B type yardangs near Daxiongshan are NNW – SSE, which are clockwise rotated compared with those in the Dalangtan area, which are elongated in a NW – SE orientation (Figure 1 and 10d). Therefore, the dominant orientation of yardangs is NW to NNE in the northwestern basin, while nearly W – E in the central eastern basin, which is consistent with previous studies, that means wind is the dominant force of yardangs formation in the Qaidam Basin.

Yardangs are separated by long, shallow troughs, where most of erosion takes place (Laity, 2011). Within the given region, the spacings, widths of these troughs, of yardangs are associated with their evolution stages. In general, yardangs with larger spacings indicate more advanced evolution stages. In the Qaidam Basin, the spacings between the W group yardangs range from 2 to 339 m, with an average value of 31 m, while those in the L group yardangs range from 4 to 76 m, with an average value of 20 m (Table 2). The narrower spacing of the L group yardangs indicates an earlier stage of evolution, relative to the W group yardangs. The troughs between yardangs may be partly or totally covered by sand ripples, mega ripples or active dunes, with axes from gentle slopes to steep slopes paralleling the long axe of yardangs and prevailing winds (Figure 3d).

4.4 Evolution processes of yardangs

Based on former studies (Brookes, 2001; Embabi, 1999; Dong et al., 2012; Halimov & Fezer, 1989) and our works, we propose a four-step (embryonic, adolescent, mature, and receding) evolution model to describe the yardangs formation and degradation in the Qaidam Basin (Figure 12).

4.4.1 Embryonic stage

During the embryonic stage, local topography low areas, e.g. tectonic fractures, depressions, or surface runoff channels, provide initial passages for wind, where wind speed is strengthened, forming the turbulence when the speed > 1 m/s (Bagnold, 1941), causing these passages to deepen, widen, and elongate along the dominate wind direction. The L group yardangs mainly form in horizontal lacustrine strata inside the basin surrounding the playas, they are characterized with relative narrow troughs and broad tops (the L-B type) in the embryonic stage. While in piedmont areas, alluvial-diluvial sediments are segmented into pieces by wind and fluvial processes forming large M-I type yardangs. Some M-I type yardangs inside the basin are controlled by pre-existing tectonic fractures. The dendritic shape M-I type yardangs are remnant steam channels, showing as positive terrains. They are protected by gravel-enriched layers, which are more resistant to wind erosion. The S-T type yardangs are developed in downwind of the folded strata (Figure 7b and 7c). Oblique topography and stratum accelerate the erosion. They form in relatively coherent sediments,

suggesting that rock property plays an important role in their formation (Halimov & Fezer, 1989; Xiao et al., 2017). Their distributions are consistent with folded stratigraphy with blunt heads orientating to upwind direction. The length of sawtooth become shortened to the upwind side. In this period, the erosion rate of the troughs is greater than the yardang bodies. Thus, during this stage most of the erosion occurs in the troughs, the height of yardangs continuously increase.

4.4.2 Adolescent stage

During the early adolescent stage, the broad heads of the L-B type yardangs are eroded into small ridges with large spacings forming the L-N type yardangs. While some of the L-B type yardangs developed in the anticline uplifts consisting of sandstone interbedded with calcareous mudstones, and marls, their broad-top are eroded into broken tops. The M-E type yardangs usually transformed from the L-B type yardangs (Figure 13e) or the M-I type yardangs (Figure 4a) under the bidirectional winds inside the basin. It is obvious that the north-south orientated L-B type yardangs were segmented by northwest wind from wind gap areas (Figure 1a and 13e). In this period, the sawtooth length continues to shorten. When the downwind areas of the S-T type yardangs are segmented by fractures (Figure 7a), rainfalls, or wind, the windward remnant parts form S-P type, W-H type, or S-R type yardangs. In the early adolescent stage, the height of the yardangs was still increasing. Meanwhile, fluvial erosion and mass wasting carve gullies surround the edge of yardangs, which provide passages for further erosion. As wind erosion continues, the height of yardangs begin to reduce, and the spacing between yardangs become larger. With leeward upper surface erosion accelerating, the L group yardangs change into many isolated W-H type yardangs that are less streamlined in shape and exhibit rough tops. In the field, the W-H type yardangs surrounding the M group yardangs (Figure 3a, 3b, and 3c), which are believed to be derived from the M-I type yardangs.

4.4.3 Mature stage

Mature stage yardangs are characterized with streamlined shape and large spacing. During this stage, troughs usually appear with flat floors and large spacings because of more resistant underlayers, and yardangs are isolated occurring, which has minimized the effects of the interference among yardang bodies in the incoming wind profile (Kerber, 2016). With erosion accelerating on the leeward upper surface and leeward corners, the W-H type yardangs are shortened in length, lowered in height, and become more streamlined, forming the W-B type yardangs. Statistics show that most of their aspect ratio values are between 2:1 and 5:1, with an average value about 3:1 (Figure 9c).

4.4.4 Receding stage

When coming to the receding stage, the W-B type yardangs continually reducing in size, forming the W-L type yardangs. They are similar in morphology, but the latter ones are much smaller than the W-H and W-B type yardangs. As wind erosion continues, their heights

are decreasing, the spacings are increasing, and finally a new erosion plain is formed before the next cycle of landscape evolution initiation.

Brookes (2001) proposed a theoretical possibility that more advanced stages occur in upwind areas. The evolution of yardangs in the Qaidam Basin appears to be cyclic. Thus, this sequence should be cyclic and varied spatially. According to previous studies (Halimov & Fezer, 1989; Li et al., 2016) and our observations, the W group yardangs were evolved from the L group yardangs. Thus, the W group yardangs should occur at the upwind of the L group yardangs. However, the L group yardangs are distributed in the upwind area in contrast to the W group yardangs in the Qaidam Basin. This situation may indicate that the L group yardang represents the beginning of the next cycle. Thus, the yardang types show us a suite of cyclic yardang evolution stages.

In addition, we must note that the evolution processes probably have been interrupted at some stages due to differences in the competence of rocks and/or the changes of environment, e.g. abrupt climate changes, tectonic movements or infilling sediments. In the Qaidam Basin, competent layers in sediments play an important role in yardangs evolution. These layers are more resistant to wind erosion, usually exhibit as "cap layers" (Figure 6b), erosion floors (troughs) (Figure 6a) or erosion plains (Figure 8f), showing flat occurrence in morphology. The next cycle may begin after the breaking of the erosion floor (e.g. planation surface). The multi-stage evolution of yardangs in the Qaidam Basin is also evident by the occurrence of overlapped yardangs (Figure 13e). As shown in figure 13e, the approximately N – S oriented early stage yardangs are segmented by subsequent NW – SE winds on their top layers, and the new forming troughs are shallower than the formers.

5 Yardangs on Mars: a comparative study

5.1 Yardangs in MFF and Gale Crater

According to the characteristics of Qaidam yardangs (Table 1), yardangs of the MFF region and Gale Crater on Mars are inspected and sorted into different types, for the purpose of comparative study.

In the MFF exposed region, we have found a large amount of dendritic-shape mesa yardangs with flat broad tops in Aeolis Dorsa (Figure 13a and 13b). They are classified into the M-I type by comparing with those in the Qaidam basin. Streamlined yardangs are developed both on their broad tops and surrounding depressions (Figure 13a). Some irregular mesa yardangs are formed in the ejecta blanket, where wind streaks are remarkable (Figure 13d). We have also identified a group of M-E type yardangs coexisting with long-ridge yardangs in the MFF area at Lucus Planum. These yardangs exhibit in NE – SW and NW – SE directions (Figure 13g), with some of them are eroded into streamlined shapes (e.g. W-B type).

Long ridge yardangs are widely spread in the MFF region. The representative L-B type yardangs analogue is in Lucus Planum (Figure 14a). They have broad tops, steep flanks, and are parallel to each other in NW – SE direction over 30 km long. Their width ranges from

10s m to ~ 1 km with height from10s m to ~290 m (Figure 14b). Some of them are eroded into narrow-top yardangs (L-N type) with double tapered ends. The northwestern part of L-B type yardangs are eroded and change into M-E or W-H type yardangs. Some L-B type paleo-yardangs are observed in northern Zephyria Planum (Figure 20e). They extended in W – E direction over 80 km and overlaid by NE – SW directional yardangs with an angle about 45 . Their widths are similar to those in Lucus Planum, while their heights are much lower (Figure 20g).

We find L-N type yardangs in Aeolis Serpens, presenting streamlined shapes with blunt heads and tapered tails. Faceted surfaces and curvilinear crestlines can be observed. Some of them are coexisting with W-H type yardangs (Figure 15a). The L-R type yardangs are extended in N – S directions in Aeolis Dorsa (Figure 15b). Their tops are quite tattered with faceted surfaces and curvilinear crestlines, and separated by broad troughs, where sand sheets are deposited in dark areas.

The S group yardangs are relatively common at the edge of layered deposits. The yardangs developed in the eastern part of Gale Crater are good analogues for the S-T type. Their stratified structures are noticeable (Figure 16b). These yardangs are developed in the thin layers and orientated to the downslope directions. Most of them have been segmented from the zigzags forming W-B or W-H type yardangs. The S-R type yardangs found at Aeolis Planum are characterized by rounded shapes (Figure 16e), which are similar in morphology with those in the Qaidam Basin (Figure 7e).

The W-B type yardangs are perfect streamlined with blunt heads and tapered tails extending in NW-SE direction in the Aeolis Planum. Their surface looks very rough (Figure 17a). Some of them show crestlines. The W-H type yardangs are widely distributed in Aeolis-Zephyria Planum (AZP). They extend in the SE-NW direction with streamlined shape and sharp crestlines. The W-H type yardangs in northern Zephyria Planum can be divided into two groups in size (Figure 17b). Their surfaces are characterized by cracks, blocks, and dark streaks (Figure 17c and 17d). Sand ripples are obvious around the yardangs, indicating that the current wind direction is consistent with the elongation of yardangs. There is no report yet about the W-L type yardangs in the MFF region due to their small sizes and data resolutions.

5.2 Comparison

Both yardangs in the Qaidam Basin on Earth and their analogues in the MFF and Gale Crater on Mars are similar in morphology according to the essential features shown in Table 1 and described above. Their characteristics are further summarized in Table 3. Here we focus on their similarities and differences in morphologies, except for those essential features listed in Table 1. The major difference between them is that most of the yardangs in the Qaidam Basin are characterized with streamlined and straight shapes except for the M group, while their analogues on Mars are evident with curvilinear crestline or faceted surfaces.

The aspect ratio values for L-B type yardangs on Mars are similar to the L group in the Qaidam Basin of which most of them are greater than 5:1 (Figure 18a), while the aspect ratio values of L-N type yardangs are between 2:1 and 20:1. The lower aspect ratios are due

to the coexisting of the L-N and W-H type yardangs in the same area (Figure 13a). The aspect ratios for the W group yardangs are concentrated between 2:1 and 4:1, with an average value of 2.5:1 (Figure 18b). The log-log plots of length versus width for yardangs both in the Qaidam Basin on Earth and their analogues on Mars show their similarity in aspect ratio values (Figure 18c), with some of yardangs in the MFF and Gale Crater on Mars much greater than their terrestrial analogues in the Qaidam Basin.

5.3 Discussion

Our morphological study shows that yardangs of the Qaidam Basin and those on Mars have large variations in shapes indicating distinct forming and evolution processes. And the observations suggest that the lithology, wind and water are the dominant controlling factors.

5.3.1 Lithology

Yardangs can be carved both in hard and soft materials under strong, unidirectional winds and their forms, scales, and rate of formation are strongly influenced by the competence of rock (Laity, 2011; McCauley et al., 1977a), which is basically controlled by the compositions and textures as those factors can affect their anti-erosion ability to wind (Dong et al., 2012). The most common and widespread formation of yardangs on Earth occurs in softer materials, notably lacustrine sediments.

In the Qaidam Basin, most of the yardangs are developed in mudstones that are easy to be eroded. Some of them (e.g. the L-N type) have “cap layers” on their surface. These “cap layers” are usually rich in gypsum crystals and showing green in color (Figure 6b). The size of these gypsum crystals can be as large as ~20 cm. These “green layers” exhibit as flat tops or surface layer (Figure 7c), indicating more resistance to wind erosion that protects the underlayers from further erosion. In addition, the gravel-enriched polygon layers (Figure 3d) and salt crusts (Figure 4d, 5, and 8) act as protectors as well. Furthermore, yardangs covered by salt crusts (e.g. the W group, Figure 8) usually display much more streamlined forms than others. Some yardangs carved in harder rocks usually exhibit irregular weathered tops (Laity, 2011), which are found in the L-R type yardangs of the Qaidam Basin that developed in sandstone interbedded with calcareous mudstones (Figure 6c).

The MFF is a light-toned friable layered deposit (e.g. Morgan et al., 2015; Tanaka, 2000; Weitz et al., 2010). Radar data suggest that the material of the MFF could be dry, low density deposits (e.g. volcanic ash) or ice-rich deposits in terms of their dielectric properties (Carter et al., 2009; Harrison et al., 2010; Head & Kreslavsky, 2001; Kerber et al., 2008; Kerber & Head, 2010, 2012; Keszthelyi & Jaeger, 2008; Watters et al., 2007). The W-H type yardangs distributed in the AZP area are evident with cracks, blocks (Figure 17c and 17d) or infrequent craters with ejected rubbles (Figure 17e), suggesting an indurated homogeneity material. These cracks and blocks maybe caused by the difference in temperature, varying greatly from day to night. However, the surface of floors seems to be rougher than the W-B type yardangs in MFF area (Figure 17a), which is similar to fluted ventifacts, implying an indurated floor layer with lateral heterogeneity. Fine layered deposits are visible on the

yardangs (Figure 17a'), indicating that the MFF materials have a multilayered structure with different competent layers, and yardangs are developed in the soft layers, which are consistent with the observations of terraced craters in MFF. Previous studies suggest that these terraced craters may be related to a subsurface ice-rich layer (e.g. Bramson et al., 2015; Kadish et al., 2009; Ormö et al., 2013).

Except for the MFF exposure area, yardangs are also found developing in the upper unit with layered sediments in Gale Crater (Le Deit et al., 2011). Thomson et al. (2011) suggests that the upper mount material may be related to the MFF material, and then supported by Zimbelman and Scheidt (2012) and Dapremont et al. (2014). The S-T type yardangs are developed in the fine layered deposits, while their surface layers look much rougher, indicating a more resistant layer (Figure 16b), which has also been found in the Qaidam Basin (Figure 16a).

5.3.2 Wind erosion

As reported in previous studies (Halimov & Fezer, 1989; Li et al., 2016; Rohrmann et al., 2013; Wei, 2013), wind is the dominant driver of yardangs erosion in the Qaidam Basin. Both the abrasion and deflation are suggested (Breed et al., 1989; Whitney, 1983), where the former plays a crucial role. Wind abrasion aids in the deepening and widening of topographic lows into troughs (Ward, 1979). It is most active within the lower 1~3 m above ground, resulting in the development of a steep, often undercut, upwind faces (Figure 19a') (Bosworth et al., 1922; Dong et al., 2004; Donner & Embabi, 2000; Grolier et al., 1980; Hobbs, 1917; Laity, 2011).

In the Qaidam Basin, moats and flank striations are observed on many steep upwind faces (Figure 4b, 17a, and 17b), indicating the dominant wind direction and turbulent erosion (McCauley et al., 1977a; Whitney, 1983). Unlike abrasion, the deflation functions across the entire surface of the yardangs all the time. In fact, these two processes always co-operate in yardang fields. However, many yardangs in the Qaidam Basin, such as the W-B type (Figure 8a), the W-L type (Figure 8f), and the L-B type yardangs (Figure 5), usually show a thick (around 50 cm), hard, salt crust, which appears to have protected the underlying horizontally layered lacustrine sediments from further wind erosion, both abrasion and deflation (Figure 8b). Dark streaks are visible in the W-H type yardangs of AZP area on Mars indicating a thick dust covering on the surface, which reveals that both the abrasion and deflation perhaps are not active in this area at present.

Most studies support that yardangs are formed by unidirectional strong wind (Hobbs, 1917; McCauley et al., 1977a; McCauley et al., 1977b; Niu et al., 2011). While opposite bidirectional winds, with one stronger, can also account for their formation (Laity, 2011; Ritley & Oontuya, 2004). Usually, the upwind side broad tops are eroded into small ridges, while their downwind areas are still unaltered, this can be used as an indicator of the prevailing wind (Figure 5b, 7b and 14c). We found the L-B type yardangs in Lucus Planum on Mars have been eroded to small ridges on both sides (Figure 14a and 14d), indicating that they have been eroded by two opposite winds. The amount of small ridges in the NW part

outnumber those in the SE part, implying that the NW wind may be stronger than the SE wind, or the NW wind worked a longer time. However, the reason why the wind changed directions during the yardangs' forming is still not clear.

In the Qaidam Basin, the M-E type yardangs develop in the downwind direction of the L group yardangs that are eroded by bidirectional winds. Their dominant long axis orientations range from NNW to N (Figure 10a), which coincides with the upwind direction of the L group yardangs (Figure 10b), and they were segmented by NW winds (Figure 13e). The angles between these two directions vary from 40° to nearly vertical. The M-E type yardangs developed in Lucus Planum on Mars also formed under bidirectional winds with angle about 80° (Figure 11g). When the angle between these two winds ranging from 30° to 45°, then usually faceted yardangs with curvilinear crestlines formed (Figure 15), which are widely distributed on the martian surface (Bradley, 2002).

In northern Zephyria Planum, yardangs developed in different layers with multiple directions are observed (Figure 20). Some L-B type paleo-yardangs are excavated to the surface with over layered L-N type yardangs (Figure 20e). Their orientation angle differences range from ~40° to ~60°, indicating the dominant wind direction changing dramatically of different periods. The variation of yardang orientations also has been found in the same layer in the east of this area (Figure 20b, 20c, and 20d). Their orientation angle differences vary from ~40° to ~60°, and the present wind directions revealed from the sand ripples are NWW – SEE. The variation of yardang orientations suggests that the dominant wind directions have changed and last for enough time to form yardangs.

5.3.3 Water erosion

Although yardangs are deemed to the result of wind erosion, water erosion occasionally exert an important influence during their evolution on Earth (Dong et al., 2012; Laity, 2011; Li et al., 2016; Wang & Ha, 2009; Wang et al., 2016; Xia, 1985; Xiao et al., 2017). For example, temporary runoff from surrounding mountains may cut the surface into pieces that provide passages to the wind. While rainfalls modify the surface of the yardangs by gullying (Figure 3b and 3d), both of which may accelerate the evolution of yardangs during the embryonic stage (Halimov & Fezer, 1989; Li et al., 2016). Water table is also an important factor. Their fluctuations can determine the depth of troughs (Laity, 2011).

The climate of Mars has become cold and dry since the Hesperian epoch (Brain & Jakosky; Carr,1999; Clifford, 1993; Ehlmann et al., 2011; Fassett & Head, 2008; Head, 2002; Golombek et al., 2006; Treiman et al., 1995; Xiao, 2013). We found some yardangs coexisting with fluvial landforms. The M-I type yardangs that developed in Aeolis Dorsa show dendritic shape (Figure 13a). In Gunjur Crater, eastern Aeolis Planum, paleo-MFF yardangs are excavated from delta deposits (Figure 21b and 21d), and remnant yardangs have also been found on the delta surface (Figure 21c), suggesting that the fluvial activity was still active during the formation or reformation of the MFF. But there is no evidence showing whether the fluvial activity has influenced the formation of yardangs.

5.3.4 Other factors

In addition to lithology, wind, and water erosion, several other factors may have also proposed to affect the formation and evolution of yardangs in the Qaidam Basin. The presence of salts in the Qaidam Basin (e.g., Dang et al., 2018) implies that salt solution and weathering may have played a significant role during yardang formation and modification. Solution features common on yardangs that are developed within playas (Figure 4d). They usually occur on the surface of leeward sides, and away from the windward abrasion areas, indicative a wetter past existed when the solution features were formed and the present drier climate has ablated the salt solution products from the windward sides (Vincent & Kattan, 2006). Mass wasting processes, very common both in the Qaidam Basin on Earth and in the MFF and Gale Crater on Mars, contribute significantly to the modification and erosion of the yardangs, which are manifested as detached boulders around the yardangs (Figure 3d and 17d).

Impact activities, in most cases, accelerate the erosion of yardangs (Figure 17e) on Mars, but the overlapping relationship between yardangs and impact structures are not common. The formation of some S-R type yardangs on Mars might also be related to the impact (Figure 16c, 16d, and 16e). It has been well demonstrated that impact cratering on competent rocks normally cause fracturing and excavation, thus decreasing the porosity of target materials (Melsoh, 1989). However, it has been recently noticed that when a target material features a high porosity, impact cratering actually causes substantial collapse of pores and melting, which decrease the porosity and enhance the strength (Scott and Wilson, 2005; Wünnemann et al., 2006). Such impact hardening occurs beneath the final crater floor, which has been used to interpret the observed larger-than-predicted gravity anomaly beneath some lunar highland impact craters (e.g., Milbury et al., 2015). For the S-R yardangs on Mars, it might be possible that preexisting impact craters that have formed within the MFF, which might have featured a high porosity (e.g. Carter et al., 2009; Ojha & Lewis, 2018; Watters et al., 2007), have caused a decrease of porosity beneath the crater floors. In this scenario, materials beneath the crater floors will be slightly stronger than the surrounding materials, thus continual weathering could cause such cone-like yardangs. When their upper layers are eroded, a streamlined yardang with blunt head and tapered tail could be formed.

5.4 Evolution processes of yardangs in the MFF and Gale Crater

Based on the evolution model of yardangs in the Qaidam Basin, several separate partial evolution processes are observed in the MFF and Gale Crater (Figure 13, 14, 15 and 16). Evidence from the crater count dating (Zimbelman, 2010; Zimbelman & Scheidt, 2012) and stratigraphy relations analysis (Kerber & Head, 2010) show that the age of the MFF material is probablyHesperian-Amazonian. During this period, the martian environment were characterized with cold, dry, extensive volcanic eruptions and ephemeral surface water (Ehlmann et al., 2011). In the early stage, the formation of the MFF interchanged with the formation the yardangs, which means that the formation of the MFF are not continuous, and wind erosion were dominant during these breaks. Then the erosions were interrupted by the

later accumulation of the MFF materials. Thus, some yardangs were probably buried by the lateral MFF materials.

The long-ridge yardangs formations were interrupted in the embryonic-adolescent stages, forming the L-B or L-N type yardangs (Figure 20). Moreover, the dominant winds were changing dramatically (Figure 20). Locally ephemeral surface water also was active, notably in the Aeolis Dorsa area (Burr et al., 2017). Then the surface water evaporated because of the dry environment, leaving numerous fluvial and alluvial sediments. With the termination of the MFF material accumulation, wind erosion dominated the MFF area and Gale Crater. Easily erodible materials were removed, leaving the dendritic mesa yardangs. With the erosion intensified, even more layers of the MFF material were removed, the paleo-yardangs were excavated to the surface (Figure 20). Then the broad tops were eroded to form small ridges, the troughs were widened, forming the L-N type yardangs (adolescent stage). With the downwind upper surface erosion accelerating, the long-ridge yardangs developed into many isolated W-H type yardangs (Figure 15a) (adolescent-mature stage). Later on, they are shortened, lowered (Figure 17b), and some of them become more streamlined W-B type yardangs (mature stage), e.g. some small streamlined yardangs were observed on the surface of M-I type yardangs (Figure 13a) and their surrounding depressions. Eventually, yardangs were removed by wind forming the plains.

In summary, yardangs in the MFF and Gale Crater have experienced similar evolution processes as those in the Qaidam Basin and they possibly have experienced a multi-stage evolution, during which the evolution processes may have been interrupted at some stages due to differences in the competence of rocks and/or changes of environment, both in the Qaidam Basin on Earth and in the MFF and Gale Crater on Mars. We need to note that a full continuous evolution sequence has not been found in our study area on Mars, indicating the regional differences of yardang evolution, which may have relation to the local wind regime, the competence of rock , and the beginning time and duration of wind erosion.

6. Conclusions

On the basis of field investigations, and high-resolution satellite and drone images, we studied the morphology, classification, and distribution of yardangs in the Qaidam Basin, analyzed their controlling factors, and discussed their evolution. We also reported potential Mars analogues, and discussed their similarities and differences in morphology and evolution mechanism. The following conclusions are drawn:

(1) The yardangs in the Qaidam Basin are mainly distributed in the central eastern and northwestern of the basin. They are classified into 11 types out of 4 main groups based on their morphologies and distributions.

(2) The average aspect ratios for the Mesa group and the whaleback group yardangs are nearly 3:1, while those for most of the long-ridge group yardangs are greater than 5:1, both in the Qaidam Basin on Earth and in the MFF and Gale Crater on Mars.

(3) Wind is probably the dominant driver of yardangs erosion in these two study areas on Earth and Mars, but water, salt, and mass wasting may also have played important roles in their formation and modification. Independent of topographic effects, the observed variation of yardangs' dominant orientations in different layers of these study areas, probably indicate a polytropic and complex wind regime when they were formed.

(4) The evolution processes of yardangs in the Qaidam Basin are divided into four stages (embryonic, adolescent, mature, and receding), which indicates a full suite of cyclic yardang evolution, although there is no full continuous four stage evolution sequence occurring in one area. The yardangs in the MFF and Gale Crater appear to have experienced a similar multi-stage evolution, during which the evolution processes may have been interrupted at some stages due to differences in the competence of rocks and/or changes of environment, e.g. the abrupt climate changes or infilling sediments.

(5) Yardangs are common landform on both Earth and Mars. Wind erosion and carving on lacustrine sediments not only indicate arid climate and wind directions, but also shed light on paleo-environments during which they formed, particularly on Mars. More in-depth studies on types, distribution, geomorphology, lithology and textures of yardangs on Mars and terrestrial analogue study are required to deepen our understanding of the paleo-environments prevailing on the planet.

Acknowledgements

We are grateful for funding from the Science and Technology Development Fund (FDCT) of Macau (Nos. 121/2017/A3, 119/2017/A3 and 107/2014/A3), National Natural Science Foundation of China (Nos. 41772050 and 41773061), MOST Special Fund from the State Key Laboratory of Geological Processes and Mineral Resources, China University of Geosciences (No. MSFGPMR05), and the Fundamental Research Funds for the Central Universities, China University of Geosciences (Wuhan) (Nos. CUGYCJH18-01 and CUG2017G02). We would like to thank Dr. Zhongping Lai for constructive discussion and suggestion. We thank Mr. Binlong Ye and Ms Ziyan Han for their help with data processing. Dr. Le Qiao, Dr. Ziye Cheng, Ms. Ting Huang, Ms. Yanan Dang, Ms. Zhuqing Xue, Mr. Limin Zhao, Mr. Yu Wei, Mr. Ping Zhu, Mr. Bo Wang, Mr. Hansheng Liu and Mr. Jiawei Zhao are thanked for fieldwork assistances.

The images used for the Qaidam Basin are from the Google Earth (https://earth.google.com/) and our field investigations. The CTX, HiRISE images, HRSC DTMs used for Mars can be downloaded at the Mars Orbital Data Explorer (http://ode.rsl.wustl.edu/mars/). CTX DTMs have been processed with the MarsSI (emars.univ-lyon1.fr) application, the MarsSI (emars.univ-lyon1.fr) application is funded by the European Union's Seventh Framework Programme (FP7/2007-2013) (ERC Grant Agreement No. 280168). All of the data used for plot in this paper can be found in the supporting information including supplemental tables and figures.

References

Anglés, A., & Li, Y. (2017). The western Qaidam Basin as a potential Martian environmental analogue: An overview. *Journal of Geophysical Research: Planets, 122*(5), 856-888. https://doi.org/10.1002/2017je005293

Bagnold, R. (1941). *The Physics of Blown Sand and Desert Dunes*. London: Chapman & Hall Ltd.

Blackwelder, E. (1934). Yardangs. *Geological Society of America Bulletin, 45*(1), 159-166. https://doi.org/10.1130/gsab-45-159

Bosworth, T. O., Woods, H., & Vaughan, T. W. (1922). *Geology of the Tertiary and Quaternary periods in the north-west part of Peru*: Macmillan and Company, limited.

Bradley, B. A. (2002). Medusae Fossae Formation: New perspectives from Mars Global Surveyor. *Journal of Geophysical Research, 107*(E8). https://doi.org/10.1029/2001je001537

Bramson, A. M., Byrne, S., Putzig, N. E., Sutton, S., Plaut, J. J., Brothers, T. C., & Holt, J. W. (2015). Widespread excess ice in Arcadia Planitia, Mars. *Geophysical Research Letters*, *42*(16), 6566-6574. https://doi:10.1002/2015GL064844

Breed, C. S., McCauley, J. F., & Whitney, M. I. (1989). Wind erosion forms. *Arid zone geomorphology*, 284-307.

Brookes, I. A. (2001). Aeolian erosional lineations in the Libyan Desert, Dakhla Region, Egypt. *Geomorphology, 39*(3-4), 189-209. https://doi.org/10.1016/s0169-555x(01)00026-5.

Burr, D., Jacobsen, R., Lefort, A., Borden, R., Boyd, A., & Peel, S. (2017). Update on Mapping of the Aeolis Dorsa Region, Mars: Discovering Ever More Diversity in This Inverted Landscape. LPI Contributions, 1986.

Carr, M. H. (2007). *The surface of Mars* (Vol. 6): Cambridge University Press.

Carter, L. M., Campbell, B. A., Watters, T. R., Phillips, R. J., Putzig, N. E., Safaeinili, A., . . . Orosei, R. (2009). Shallow radar (SHARAD) sounding observations of the Medusae Fossae Formation, Mars. *Icarus, 199*(2), 295-302. https://doi.org/10.1016/j.icarus.2008.10.007

Chamberlain, T. E., Cole, H. L., Dutton, R. G., Greene, G. C., & Tillman, J. E. (1976). Atmopspheric Measurements on Mars: the Viking Meteorology Experiment. *Bulletin of the American Meteorological Society, 57*(9), 1094-1104. https://doi.org/10.1175/1520-0477(1976)057<1094:amomtv>2.0.co;2

Dang, Y. N., Xiao, L., Xu, Y., Zhang, F., Huang, J., Wang, J., ... & Yue, Z. Y. (2018). The Polygonal Surface Structures in the Dalangtan Playa, Qaidam Basin, NW China: Controlling Factors for their Formation and Implications for Analogous Martian Landforms. *Journal of Geophysical Research: Planets*. https://doi.org/10.1029/2018JE005525

Dapremont, A., Allen, C., & Runyon, C. (2014). *The Gale Crater Mound in a Regional Geologic Setting: Comparison Study of Wind Erosion in Gale Crater and Within a 1000 km Radius*. Paper presented at the Lunar and Planetary Science Conference.

Day, M., & Kocurek, G. (2016). Observations of an aeolian landscape: From surface to orbit in Gale Crater. *Icarus, 280*, 37-71. https://doi.org/10.1016/j.icarus.2015.09.042

Desai, A. J., & Murty, S. V. S. (2016). Morphology of Yardangs Within Nicholson Crater, Mars: Records of Past Fluvial and Aeolian Activities. *Journal of the Indian Society of Remote Sensing, 44*(6), 933-948. https://doi.org/10.1007/s12524-016-0570-9

Dong, Z., Lv, P., Lu, J., Qian, G., Zhang, Z., & Luo, W. (2012). Geomorphology and origin of Yardangs in the Kumtagh Desert, Northwest China. *Geomorphology, 139-140*, 145-154. https://doi.org/10.1016/j.geomorph.2011.10.012

Dong, Z., Wang, H., Liu, X., & Wang, X. (2004). A wind tunnel investigation of the influences of fetch length on the flux profile of a sand cloud blowing over a gravel surface. *Earth Surface Processes and Landforms, 29*(13), 1613-1626. https://doi.org/10.1002/esp.1116

Donner, J., & Embabi, N. S. (2000). The significance of yardangs and ventifacted rock outcrops in the reconstruction of changes in the late Quaternary wind regime in the western desert of Egypt [L'importance des yardangs et des affleurements de roches modelées par le vent dans la reconstitution des changements du régime des vents au Quaternaire supérieur dans le désert libyque, Egypte]. *Quaternaire, 11*(3), 179-185. https://doi.org/10.3406/quate.2000.1667

Ehlmann, B. L., Mustard, J. F., Murchie, S. L., Bibring, J. P., Meunier, A., Fraeman, A. A., & Langevin, Y. (2011). Subsurface water and clay mineral formation during the early history of Mars. *Nature, 479*(7371), 53-60. https://doi.org/10.1038/nature10582

Embabi, N. (1999). Playas of the western desert, Egypt. *Studies of playas in the Western Desert of Egypt*, 5-47.

Fairén, A. G., Stokes, C. R., Davies, N. S., Schulze-Makuch, D., Rodríguez, J. A. P., Davila, A. F., . . . Squyres, S. W. (2014). A cold hydrological system in Gale crater, Mars. *Planetary and Space Science, 93-94*, 101-118. https://doi.org/10.1016/j.pss.2014.03.002

Fan, X. (1962). Geomorphology of Northwestern Qaidam Basin near Lenghu. *Acta Geographica Sinica, 28*(4), 15.

Fang, X., Zhang, W., Meng, Q., Gao, J., Wang, X., King, J., . . . Miao, Y. (2007). High-resolution magnetostratigraphy of the Neogene Huaitoutala section in the eastern Qaidam Basin on the NE Tibetan Plateau, Qinghai Province, China and its implication on tectonic uplift of the NE Tibetan Plateau. *Earth and Planetary Science Letters, 258*(1-2), 293-306. https://doi.org/10.1016/j.epsl.2007.03.042

Fassett, C. I., & Head, J. W. (2008). Valley network-fed, open-basin lakes on Mars: Distribution and implications for Noachian surface and subsurface hydrology. *Icarus, 198*(1), 37-56. https://doi.org/10.1016/j.icarus.2008.06.016

Fox, R. W., & McDonald, A. T. (1973). *Introduction to fluid mechanics*: John Wiley & Sons New York.

Goudie, A. (1989). Wind erosion in deserts. *Proceedings of the Geologists' Association, 100*(1), 83-92.

Goudie, A. S. (2007). Mega-Yardangs: A Global Analysis. *Geography Compass, 1*(1), 65-81. https://doi.org/10.1111/j.1749-8198.2006.00003.x

Greeley, R., Arvidson, R. E., Elachi, C., Geringer, M. A., Plaut, J. J., Saunders, R. S., . . . Weitz, C. M. (1992). Aeolian features on Venus: Preliminary Magellan results. *Journal of Geophysical Research, 97*(E8), 13319. https://doi.org/10.1029/92je00980

Greeley, R., & Iversen, J. D. (1987). *Wind as a geological process: on Earth, Mars, Venus and Titan* (Vol. 4): CUP Archive.

Grolier, M. J., McCauley, J. F., Breed, C. S., & Embabi, N. S. (1980). Yardangs of the Western Desert. *The Geographical Journal, 146*(1), 86. https://doi.org/10.2307/634077

Grotzinger, J. P., Sumner, D. Y., Kah, L., Stack, K., Gupta, S., Edgar, L., . . . Mangold, N. (2014). A habitable fluvio-lacustrine environment at Yellowknife Bay, Gale Crater, Mars. *science, 343*(6169), 1242777. https://doi:10.1126/science.1242777.

Hörner, N. G. (1932). Lop-Nor: Topographical and Geological Summary. *Geografiska Annaler, 14*(3-4), 297-321. https://doi.org/10.1080/20014422.1932.11880554

Halimov, M., & Fezer, F. (1989). Eight yardang types in Central-Asia. *Zeitschrift fur Geomorphologie, 33*(2), 205-217.

Han, W., Ma, Z., Lai, Z., Appel, E., Fang, X., & Yu, L. (2014). Wind erosion on the north-eastern Tibetan Plateau: constraints from OSL and U-Th dating of playa salt crust in the Qaidam Basin. *Earth Surface Processes and Landforms, 39*(6), 779-789. https://doi.org/10.1002/esp.3483

Harrison, S. K., Balme, M. R., Hagermann, A., Murray, J. B., & Muller, J. P. (2010). Mapping Medusae Fossae Formation materials in the southern highlands of Mars. *Icarus, 209*(2), 405-415. https://doi.org/10.1016/j.icarus.2010.04.016

Head, J., & Kreslavsky, M. A. (2001). *Medusae Fossae Formation as volatile-rich sediments deposited during high obliquity: An hypothesis and tests.* Paper presented at the Conference on the Geophysical Detection of Subsurface Water on Mars.

Head, J. W. (2002). Northern lowlands of Mars: Evidence for widespread volcanic flooding and tectonic deformation in the Hesperian Period. *Journal of Geophysical Research, 107*(E1). https://doi.org/10.1029/2000je001445

Hedin, S. A. (1903). *Central Asia and Tibet* (Vol. 1): Hurst and Blackett, limited.

Hobbs, W. H. (1917). The Erosional and Degradational Processes of Deserts, with Especial Reference to the Origin of Desert Depressions. *Annals of the Association of American Geographers, 7*(1), 25-60. https://doi.org/10.1080/00045601709357054

Hu, C., Chen, N., Kapp, P., Chen, J., Xiao, A., & Zhao, Y. (2017). Yardang geometries in the Qaidam Basin and their controlling factors. *Geomorphology, 299*, 142-151. https://doi.org/10.1016/j.geomorph.2017.09.029

Hu, D. (1990). Geomorphology of Qarhan Salt Lakes. *Journal of Lake Science*(01), 37-43.

Huang, Q., Huang, H., & Ma, Y. (1996). *Geology of Qaidam Basin and its petroleum prediction: stereo-geology, 3-D stress, oil-accumulation model*: Geological Publishing House.

Hurowitz, J. A., Grotzinger, J. P., Fischer, W. W., McLennan, S. M., Milliken, R. E., Stein, N., ... & Fairen, A. G. (2017). Redox stratification of an ancient lake in Gale crater, Mars. *Science, 356*(6341), eaah6849.

Kadish, S. J., Barlow, N. G., & Head, J. W. (2009). Latitude dependence of Martian pedestal craters: Evidence for a sublimation-driven formation mechanism. *Journal of Geophysical Research: Planets, 114*(E10). https://doi:10.1029/2008je003318

Kapp, P., Pelletier, J. D., Rohrmann, A., Heermance, R., Russell, J., & Ding, L. (2011). Wind erosion in the Qaidam basin, central Asia: Implications for tectonics, paleoclimate, and the source of the Loess Plateau. *GSA Today, 21*(4), 4-10. https://doi.org/10.1130/gsatg99a.1

Kerber, L., Head, J., Madeleine, J., Wilson, L., & Forget, F. (2008). *Modeling ash dispersal from Apollinaris Patera: implications for the Medusae Fossae formation.* Paper presented at the Lunar and Planetary Science Conference.

Kerber, L., & Head, J. W. (2010). The age of the Medusae Fossae Formation: Evidence of Hesperian emplacement from crater morphology, stratigraphy, and ancient lava contacts. *Icarus, 206*(2), 669-684. https://doi.org/10.1016/j.icarus.2009.10.001

Kerber, L., Head, J. W., Madeleine, J.-B., Forget, F., & Wilson, L. (2011). The dispersal of pyroclasts from Apollinaris Patera, Mars: Implications for the origin of the Medusae Fossae Formation. *Icarus, 216*(1), 212-220. https://doi:10.1016/j.icarus.2011.07.035

Kerber, L., & Head, J. W. (2012). A progression of induration in Medusae Fossae Formation transverse aeolian ridges: evidence for ancient aeolian bedforms and extensive reworking. *Earth Surface Processes and Landforms, 37*(4), 422-433. https://doi.org/10.1002/esp.2259

Kerber, L. (2016). *Controls on the Morphology of Yardangs on the Earth and Mars*. Paper presented at the Lunar and Planetary Science Conference.

Keszthelyi, L., & Jaeger, W. (2008). *HiRISE observations of the Medusae Fossae formation.* Paper presented at the Lunar and Planetary Science Conference.

Kieffer, H. H., Martin, T. Z., Peterfreund, A. R., Jakosky, B. M., Miner, E. D., & Palluconi, F. D. (1977). Thermal and albedo mapping of Mars during the Viking primary mission. *Journal of Geophysical Research, 82*(28), 4249-4291. https://doi.org/10.1029/JS082i028p04249

Kite, E. S., Lewis, K. W., Lamb, M. P., Newman, C. E., & Richardson, M. I. (2013). Growth and form of the mound in Gale Crater, Mars: Slope wind enhanced erosion and transport. *Geology, 41*(5), 543-546. https://doi.org/10.1130/g33909.1

Kong, F. J. K., W. G.; Hu, B.; Zheng, M. P. (2013). *Meterological Data, Surface Temperature and Moisture Conditions at the Dalantan Mars Analogous Site, in Qinghaitibet Plateau, China*. Paper presented at the Lunar and Planetary Science Conference, 1743, 1719.

Kong, F., Zheng, M., Hu, B., Wang, A., Ma, N., & Sobron, P. (2018). Dalangtan Saline Playa in a Hyperarid Region on Tibet Plateau-I: Evolution and Environments. *Astrobiology*.

https://doi.org/10.1089/ast.2018.1830

Krinsley, D. B. (1970). *A Geomorphological and Paleoclimatological Study of the Playas of Iran.* . Retrieved from

Laity, J. E. (2011). Wind erosion in drylands. *Arid Zone Geomorphology: Process, Form and Change in Drylands, Third Edition*, 539-568.

Le Deit, L., Hauber, E., Fueten, F., Pondrelli, M., Rossi, A., Mangold, N., . . . Jaumann, R. (2011). *Geological analysis of Gale Crater on Mars.* Paper presented at the EPSC-DPS Joint Meeting 2011.

Le Deit, L., Hauber, E., Fueten, F., Pondrelli, M., Rossi, A. P., & Jaumann, R. (2013). Sequence of infilling events in Gale Crater, Mars: Results from morphology, stratigraphy, and mineralogy. *Journal of Geophysical Research: Planets, 118*(12), 2439-2473. https://doi.org/10.1002/2012je004322

Li, J., & Dong, Z. (2011). Morphological Parameters of Yardangs in Southeastern Qaidam Basin. *Bulletin of Soil and Water Conservation, 31*(04), 122-125.

Li, J., Dong, Z., Li, E., & Yang, N. (2013). Wind Regime of Yardang Landform Regions in the Qarhan Salt Lake. *Journal of Desert Research*(05), 1293-1298.

Li, J., Dong, Z., Qian, G., Zhang, Z., Luo, W., Lu, J., & Wang, M. (2016). Yardangs in the Qaidam Basin, northwestern China: Distribution and morphology. *Aeolian Research, 20*, 89-99. https://doi.org/10.1016/j.aeolia.2015.11.002

Li, L., Dong, Z., Li, C., Cui, X., Xiao, W., & Xiao, N. (2018). Camparison of Yardang Morphology on the Earth and the Mars: taking the Elysium Planitia and theQaidam Basin for an example. *Journal of Desert Research, 38*(4), 08. https://doi.org/10.7522/j.issn. 1000-694X.2017.00046

Li, M., Fang, X., Yi, C., Gao, S., Zhang, W., & Galy, A. (2010). Evaporite minerals and geochemistry of the upper 400m sediments in a core from the Western Qaidam Basin, Tibet. *Quaternary International, 218*(1-2), 176-189. https://doi.org/10.1016/j.quaint.2009.12.013

Malin, M. C., Bell, J. F., Cantor, B. A., Caplinger, M. A., Calvin, W. M., Clancy, R. T., . . . Wolff, M. J. (2007). Context Camera Investigation on board the Mars Reconnaissance Orbiter. *Journal of Geophysical Research, 112*(E5). https://doi.org/10.1029/2006je002808

Mandt, K., Silva, S. d., Zimbelman, J., & Wyrick, D. (2009). Distinct erosional progressions in the Medusae Fossae Formation, Mars, indicate contrasting environmental conditions. *Icarus, 204*(2), 471-477. https://doi:10.1016/j.icarus.2009.06.031

Mandt, K. E., de Silva, S. L., Zimbelman, J. R., & Crown, D. A. (2008). Origin of the Medusae Fossae Formation, Mars: Insights from a synoptic approach. Journal of *Geophysical Research: Planets, 113*(E12). https://doi:doi.org/10.1029/2008JE003076

McCauley, J., Grolier, M., & Breed, C. (1977). Yardangs. *Geomorphology in arid regions*, 233-269.

McCauley, J. F., Grolier, M. J., & Breed, C. S. (1977). *Yardangs of Peru and other desert regions*: US Geological Survey.

McEwen, A. S., Eliason, E. M., Bergstrom, J. W., Bridges, N. T., Hansen, C. J., Delamere, W. A., . . . Weitz, C. M. (2007). Mars Reconnaissance Orbiter's High Resolution Imaging Science Experiment (HiRISE). *Journal of Geophysical Research, 112*(E5). https://doi.org/10.1029/2005je002605

Melosh, H. J. (1989). *Impact cratering: A geologic process*. Research supported by NASA. New York, Oxford University Press (Oxford Monographs on Geology and Geophysics, No. 11), 1989, 253 p., 11.

Milbury, C., Johnson, B. C., Melosh, H. J., Collins, G. S., Blair, D. M., Soderblom, J. M., & Zuber, M. T. (2015). The effect of pre-impact porosity on the gravity signature of lunar craters. *Lunar Planet. Sci, 46*

Milliken, R., Grotzinger, J., & Thomson, B. (2010). Paleoclimate of Mars as captured by the stratigraphic record in Gale Crater. *Geophysical Research Letters, 37*(4). https://doi:10.1029/2009GL041870

Moratto, Z., Broxton, M., Beyer, R., Lundy, M., & Husmann, K. (2010). *Ames Stereo Pipeline, NASA's open source automated stereogrammetry software.* Paper presented at the Lunar and Planetary Science Conference.

Morgan, G. A., Campbell, B. A., Carter, L. M., & Plaut, J. J. (2015). Evidence for the episodic erosion of the Medusae Fossae Formation preserved within the youngest volcanic province on Mars. *Geophysical Research Letters, 42*(18), 7336-7342. https://doi.org/10.1002/2015gl065017

Niu, H., Qu, J., Li, X., Dong, G., Zhang, K., & Han, Q. (2011). Review and Prospect of Yardangs Landforms Research. *Advances in Earth Science, 26*(05), 516-527.

Ojha, L., & Lewis, K. (2018). The Density of the Medusae Fossae Formation: Implications for its Composition, Origin, and Importance in Martian History. *Journal of Geophysical Research: Planets*. https://doi.org/10.1029/2018JE005565

Ormö, J., Rossi, A. P., & Housen, K. R. (2013). A new method to determine the direction of impact: Asymmetry of concentric impact craters as observed in the field (Lockne), on Mars, in experiments, and simulations. *Meteoritics & Planetary Science, 48*(3), 403-419. https://doi:10.1111/maps.12065

Paillou, P., & Radebaugh, J. (2013). *Looking for Mega-Yardangs on Titan: A Comparative Planetology Approach.* Paper presented at the European Planetary Science Congress 2013, held 8-13 September in London, UK. Online at: http://meetings. copernicus. org/epsc2013, id. EPSC2013-85.

Read, P. L., & Lewis, S. R. (2004). *The Martian climate revisited: atmosphere and environment of a desert planet.* Springer Science & Business Media.

Ren, J. (1996). Physical geographical characteristics of Qaidam region. *Journal of Qinghai*

Environment, 21(03), 149-150.

Reshetyuk, Y., & Mårtensson, S.-G. (2016). Generation of Highly Accurate Digital Elevation Models with Unmanned Aerial Vehicles. *The Photogrammetric Record, 31*(154), 143-165. https://doi.org/10.1111/phor.12143

Ritley, M. K., & Oontuya, E. (2004). *Yardangs and dome dunes northeast of Tavan Har, Gobi, Mongolia.* Paper presented at the GSA Abstracts with Programs.

Rohrmann, A., Heermance, R., Kapp, P., & Cai, F. (2013). Wind as the primary driver of erosion in the Qaidam Basin, China. *Earth and Planetary Science Letters, 374*, 1-10. https://doi.org/10.1016/j.epsl.2013.03.011

Scott, D. H., & Tanaka, K. L. (1986). Geologic map of the western equatorial region of Mars: Geological Survey (US).

Scott, E. R., & Wilson, L. (2005). Meteoritic and other constraints on the internal structure and impact history of small asteroids. *Icarus*, 174(1), 46-53. https://doi.org/10.1016/j.icarus.2004.10.014

Stack, K. M., Edwards, C., Grotzinger, J., Gupta, S., Sumner, D., Calef, F., . . . Jacob, S. (2016). Comparing orbiter and rover image-based mapping of an ancient sedimentary environment, Aeolis Palus, Gale crater, Mars. *Icarus, 280*, 3-21. https://doi:10.1016/j.icarus.2016.02.024

Tanaka, K. (2000). Dust and Ice Deposition in the Martian Geologic Record. *Icarus, 144*(2), 254-266. https://doi.org/10.1006/icar.1999.6297

Tanaka, K. L., Robbins, S. J., Fortezzo, C. M., Skinner, J. A., & Hare, T. M. (2014). The digital global geologic map of Mars: Chronostratigraphic ages, topographic and crater morphologic characteristics, and updated resurfacing history. *Planetary and Space Science, 95*, 11-24. https://doi.org/10.1016/j.pss.2013.03.006

Tapponnier, P., Zhiqin, X., Roger, F., Meyer, B., Arnaud, N., Wittlinger, G., & Jingsui, Y. (2001). Oblique stepwise rise and growth of the Tibet plateau. *science, 294*(5547), 1671-1677. https://doi.org/10.1126/science.105978

Thomson, B. J., Bridges, N. T., Milliken, R., Hook, S., Baldridge, A., Crowley, J., & Marion, G. (2008, December). Signs of aqueous activity in Gale Crater, Mars as viewed by Mars Reconnaissance Orbiter. *In AGU Fall Meeting Abstracts*.

Thomson, B. J., Bridges, N. T., Milliken, R., Baldridge, A., Hook, S. J., Crowley, J. K., . . . Weitz, C. M. (2011). Constraints on the origin and evolution of the layered mound in Gale Crater, Mars using Mars Reconnaissance Orbiter data. *Icarus, 214*(2), 413-432. https://doi.org/10.1016/j.icarus.2011.05.002

Vincent, P., & Kattan, F. (2006). Yardangs on the Cambro-Ordovician Saq Sandstones, North-West Saudi Arabia. *Zeitschrift für Geomorphologie, NF*, 305-320. https://doi.org/10.1127/zfg/50/2006/305

Viúdez-Moreiras, D., Gómez-Elvira, J., Newman, C., Navarro, S., & Marin, M. (2017). *Gale Wind Speed Weibull Distribution Based on the First Two Years of REMS Wind Data*. Paper

presented at the Sixth International Workshop on the Mars Atmosphere: Modelling and observation, Granada, Spain. .

Wang, E., Xu, F. Y., Zhou, J. X., Wan, J., & Burchfiel, B. C. (2006). Eastward migration of the Qaidam basin and its implications for Cenozoic evolution of the Altyn Tagh fault and associated river systems. *Geological Society of America Bulletin, 118*(3-4), 349-365. https://doi.org/10.1130/b25778.1

Wang, J., Fang, X., Appel, E., & Song, C. (2012b). Pliocene-Pleistocene Climate Change At the NE Tibetan Plateau Deduced From Lithofacies Variation In the Drill Core SG-1, Western Qaidam Basin, China. *Journal of Sedimentary Research, 82*(12), 933-952. https://doi.org/10.2110/jsr.2012.76

Wang, S., & Ha, S. (2009). Advances in the Study of Geomorphology and Process of Wind Erosion Landforms. *Journal of Earth Sciences and Environment*, (01), 100-105.

Wang, Y., Wu, F., Zhang, X., Zeng, P., Ma, P., Song, Y., & Chu, H. A. O. (2016). Formation and evolution of yardangs activated by Late Pleistocene tectonic movement in Dunhuang, Gansu Province of China. *Journal of Earth System Science, 125*(8), 1603-1614. https://doi.org/10.1007/s12040-016-0749-z

Wang, Y., Zheng, J., Zhang, W., Li, S., Liu, X., Yang, X., & Liu, Y. (2012a). Cenozoic uplift of the Tibetan Plateau: Evidence from the tectonic–sedimentary evolution of the western Qaidam Basin. *Geoscience Frontiers, 3*(2), 175-187. https://doi.org/10.1016/j.gsf.2011.11.005

Ward, A. W. (1979). Yardangs on Mars: Evidence of recent wind erosion. *Journal of Geophysical Research, 84*(B14), 8147. https://doi.org/10.1029/JB084iB14p08147

Ward, A. W., Doyle, K. B., Helm, P. J., Weisman, M. K., & Witbeck, N. E. (1985). Global map of eolian features on Mars. *Journal of Geophysical Research, 90*(B2), 2038. https://doi.org/10.1029/JB090iB02p02038

Ward, A. W., & Greeley, R. (1984). Evolution of the yardangs at Rogers Lake, California. *Geological Society of America Bulletin, 95*(7), 829. https://doi.org/10.1130/0016-7606(1984)95<829:eotyar>2.0.co;2

Watters, T. R., Campbell, B., Carter, L., Leuschen, C. J., Plaut, J. J., Picardi, G., . . . Stofan, E. R. (2007). Radar sounding of the Medusae Fossae Formation Mars: equatorial ice or dry, low-density deposits? *science, 318*(5853), 1125-1128. https://doi.org/10.1126/science.1148112

Wei, K. (2013). Study on Open Terme Rick Mine Landform Evolution Model and Morphological Differences. *Science Technology and Engineering* (33), 9908-9912.

Weitz, C. M., Milliken, R. E., Grant, J. A., McEwen, A. S., Williams, R. M. E., Bishop, J. L., & Thomson, B. J. (2010). Mars Reconnaissance Orbiter observations of light-toned layered deposits and associated fluvial landforms on the plateaus adjacent to Valles Marineris. *Icarus, 205*(1), 73-102. https://doi.org/10.1016/j.icarus.2009.04.017

Whitney, M. I. (1983). Eolian Features Shaped by Aerodynamic and Vorticity Processes. *Developments in Sedimentology, 38*, 223-245. https://doi.org/10.1016/s0070-4571(08)70797-0

Wu, G., Hu, S., Zhang, Z., Zhao, H., & Fang, X. (1985). The Qaidam Basin. *Journal of Lanzhou University(natural science), 1985*, 60-63.

Wu, Z. (2009). *Deserts and Desertification Control in China.* Beijing: Science Press, 714.

Wu, Z., Yang, Y., Barosh, P. J., Wu, Z., & Zhang, Y. (2014). Tectonics and Topography of the Tibetan Plateau in Early Miocene. *Acta Geologica Sinica - English Edition, 88*(2), 410-424. https://doi.org/10.1111/1755-6724.12205

Wünnemann, K., Collins, G. S., & Melosh, H. J. (2006). A strain-based porosity model for use in hydrocode simulations of impacts and implications for transient crater growth in porous targets. *Icarus*, 180(2), 514-527. https://doi.org/10.1016/j.icarus.2005.10.013

Xia, W., Zhang, N., Yuan, X., Fan, L., & Zhang, B. (2001). Cenozoic Qaidam basin, China: A stronger tectonic inversed, extensional rifted basin. *AAPG bulletin, 85*(4), 715-736. https://doi.org/10.1306/8626c98d-173b-11d7-8645000102c1865d

Xia, X. (1985). Review to the Scientific Ivestigation in Lop Nor, Xinjiang. *Arid Zone Research, 1*, 1-5.

Xia, X. (1987). *The cause of yardangs landform in Lor Nor region*. Beijing: Sciences Press.

Xiao, L. (2013). *Planetary Geology*. Beijing: Geological Publishing House.

Xiao, L., Wang, J., Dang, Y., Cheng, Z., Huang, T., Zhao, J., . . . Komatsu, G. (2017). A new terrestrial analogue site for Mars research: The Qaidam Basin, Tibetan Plateau (NW China). *Earth-Science Reviews, 164*, 84-101. https://doi.org/10.1016/j.earscirev.2016.11.003

Yang, J., Xu, Z., Zhang, J., Chu, C.-Y., Zhang, R., & Liou, J.-G. (2001). Tectonic significance of early Paleozoic high-pressure rocks in Altun-Qaidam-Qilian Mountains, northwest China. *Memoirs-Geological Society of America*, 151-170.

Yang, G. (2009). On Distribution of the Yardang in Xinjiang. *Acta Geologica Sichuan*, S2.

Yin, A., Dang, Y. Q., Wang, L. C., Jiang, W. M., Zhou, S. P., Chen, X. H., . . . McRivette, M. W. (2008). Cenozoic tectonic evolution of Qaidam basin and its surrounding regions (Part 1): The southern Qilian Shan-Nan Shan thrust belt and northern Qaidam basin. *Geological Society of America Bulletin, 120*(7-8), 813-846. https://doi.org/10.1130/b26180.1

Yin, A., Manning, C. E., Lovera, O., Menold, C. A., Chen, X., & Gehrels, G. E. (2007). Early Paleozoic Tectonic and Thermomechanical Evolution of Ultrahigh-Pressure (UHP) Metamorphic Rocks in the Northern Tibetan Plateau, Northwest China. *International Geology Review, 49*(8), 681-716. https://doi.org/10.2747/0020-6814.49.8.681

Yin, A., Rumelhart, P. E., Butler, R., Cowgill, E., Harrison, T. M., Foster, D. A., . . . Raza, A. (2002). Tectonic history of the Altyn Tagh fault system in northern Tibet inferred from Cenozoic sedimentation. *Geological Society of America Bulletin, 114*(10), 1257-1295. https://doi.org/10.1130/0016-7606(2002)114<1257:thotat>2.0.co;2

Zaki, A. S. (2016). *Morphology and Sedimentology of Landforms Associated with Playas in Western Desert of Egypt: Possible Analogs for Mars.* Paper presented at the Lunar and

Planetary Science Conference.

Zhang, J., & Liu, E. (1985). Hydrological Characteristics of Streams in Qaidam Basin. *Journal of Geographical Sciences*(03), 242-255.

Zhang, P. Z., Shen, Z., Wang, M., Gan, W., Bürgmann, R., Molnar, P., ... & Hanrong, S. (2004). Continuous deformation of the Tibetan Plateau from global positioning system data. *Geology*, 32(9), 809-812. https://doi.org/10.1130/G20554.1

Zhang, W., Appel, E., Fang, X., Song, C., & Cirpka, O. (2012). Magnetostratigraphy of deep drilling core SG-1 in the western Qaidam Basin (NE Tibetan Plateau) and its tectonic implications. *Quaternary Research, 78*(1), 139-148. https://doi.org/10.1016/j.yqres.2012.03.011

Zhang, W., Fang, X., Song, C., Appel, E., Yan, M., & Wang, Y. (2013). Late Neogene magnetostratigraphy in the western Qaidam Basin (NE Tibetan Plateau) and its constraints on active tectonic uplift and progressive evolution of growth strata. *Tectonophysics, 599*, 107-116. https://doi.org/10.1016/j.tecto.2013.04.010

Zheng, M., Wang, A., Kong, F., & Ma, N. (2009). *Saline lakes on Qinghai-Tibet Plateau and salts on Mars.* Paper presented at the Lunar and Planetary Science Conference, XL, Abstract.

Zhong, J., Wen, Z., Guo, Z., Wang, H., & Gao, J. (2004). Paleogene and early neogene lacustrine reefs in the western qaidam basin, china. *Acta Geologica Sinica, 78*(3), 736-743.

Zimbelman, J. (2010). *Geologic Mapping of the Medusae Fossae Formation, Mars, and the Northern Lowland Plains, Venus*. Paper presented at the Lunar and Planetary Science Conference.

Zimbelman, J. R., & Griffin, L. J. (2010). HiRISE images of yardangs and sinuous ridges in the lower member of the Medusae Fossae Formation, Mars. *Icarus, 205*(1), 198-210. https://doi:10.1016/j.icarus.2009.04.003

Zimbelman, J. R., & Scheidt, S. P. (2012). Hesperian age for western medusae fossae formation, Mars. *science, 336*(6089), 1683-1683. https://doi:10.1126/science.1221094

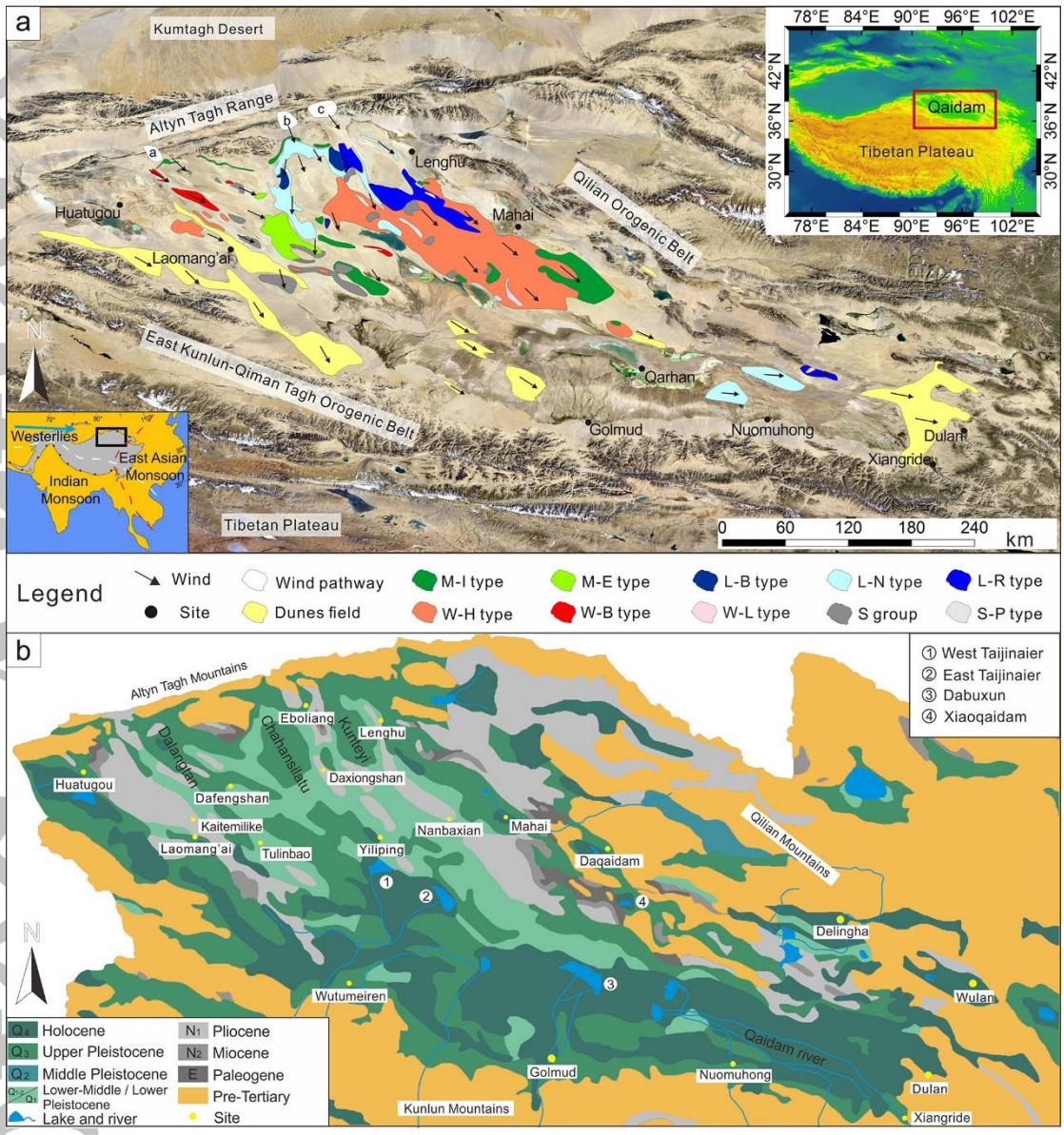

Figure 1. (a) The Qaidam Basin and distributions of different yardang fields. Black solid arrows mark the dominant wind direction shown in Kapp et al. (2011). **(b)** Simplified geological map of the Qaidam Basin (after Li et al., 2016).

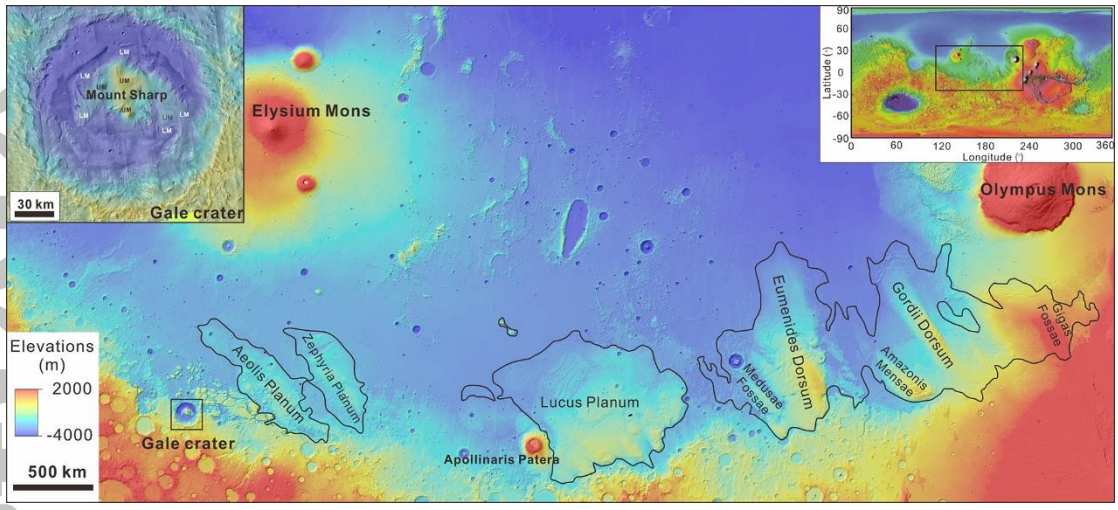

Figure 2. Location of the MFF exposure area (black outlines) and Gale Crater (black box), using MOLA topography overlaid onto a hillshade (4X exaggerate in height, modified after Kerber et al., 2011). The Upper member (UM) and Lower member are marked in the inset figure.

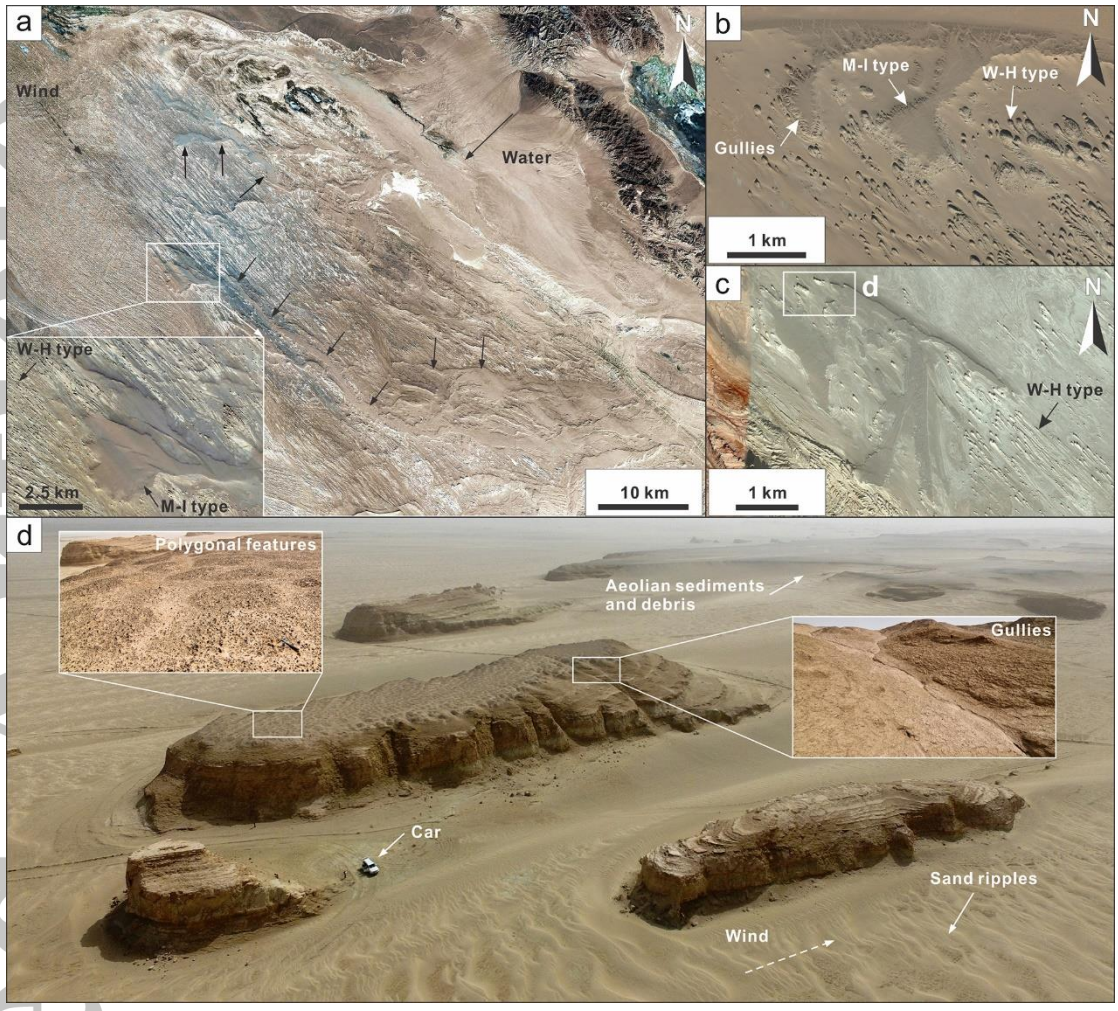

Figure 3. The irregular mesa (M-I type) yardangs in the Qaidam Basin. **(a)** The M-I type yardangs between Mahai and Xiaoqaidam (black arrows mark the position of some M-I type yardangs, image center: 37.70° N, 94.69° E). **(b)** The M-I type yardangs in the north of Dabuxun Lake (37.25° N, 95.10° E). Some M-I type yardangs have transformed into W-H type yardangs. **(c)** The M-I type yardangs in the southeast of Lenghu (38.46° N, 93.45° E). **(d)** The M-I type yardangs in the southeast of Lenghu (38.46° N, 93.43° E). Sand ripples indicate the wind direction. Gullies and polygonal features are found on the M-I type yardangs.

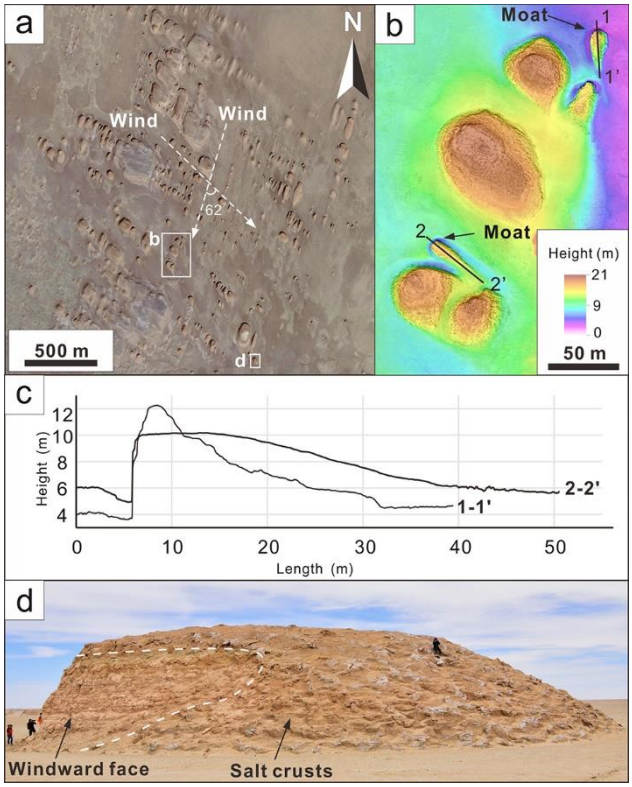

Figure 4. The elongated mesa (M-E type) yardangs in the Qaidam Basin. **(a)** The M-E type yardangs in the bidirectional area (white dashed arrows indicate two wind directions, image center: 38.07° N, 92.14° E). **(b)** DTM superposed on drone images of the M-E type yardangs shown in **(a)**. Clearly visible are moats surrounding the upwind heads of the yardangs. **(c)** The profiles of yardang 1 and yardang 2 in **(b)**. Black lines mark the location of the profiles. The moat in site 2 is deeper than that in site 1. **(d)** The M-E type yardangs with an eroded windward face (white dashed line marks the boundary) shown in (**a**).

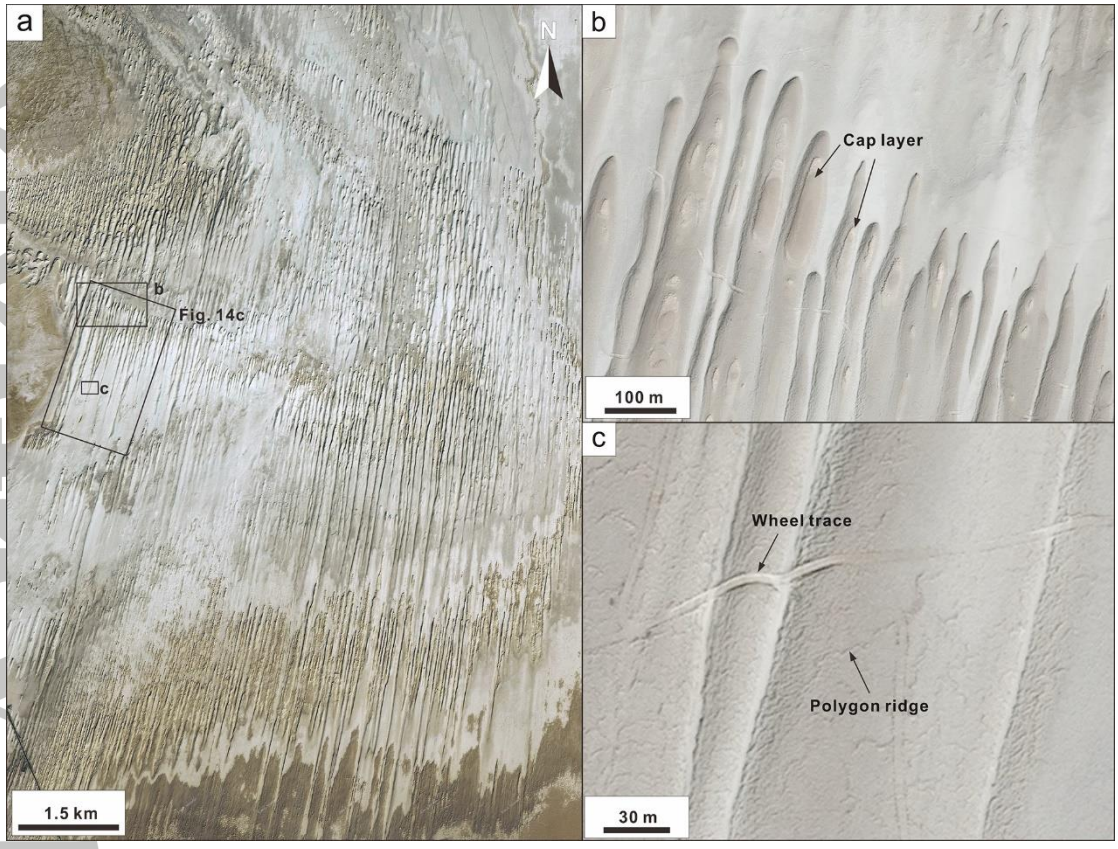

Figure 5. The broad-top long-ridge (L-B type) yardangs in the Qaidam Basin. **(a)** L-B type yardangs in the western Qarhansilatu playa (38.49° N, 92.26° E). **(b)** The heads of the L-B type yardangs are eroded into small ridges, some remnant cap rocks are on the surface. **(c)** Large polygons developed on the surface of yardangs.

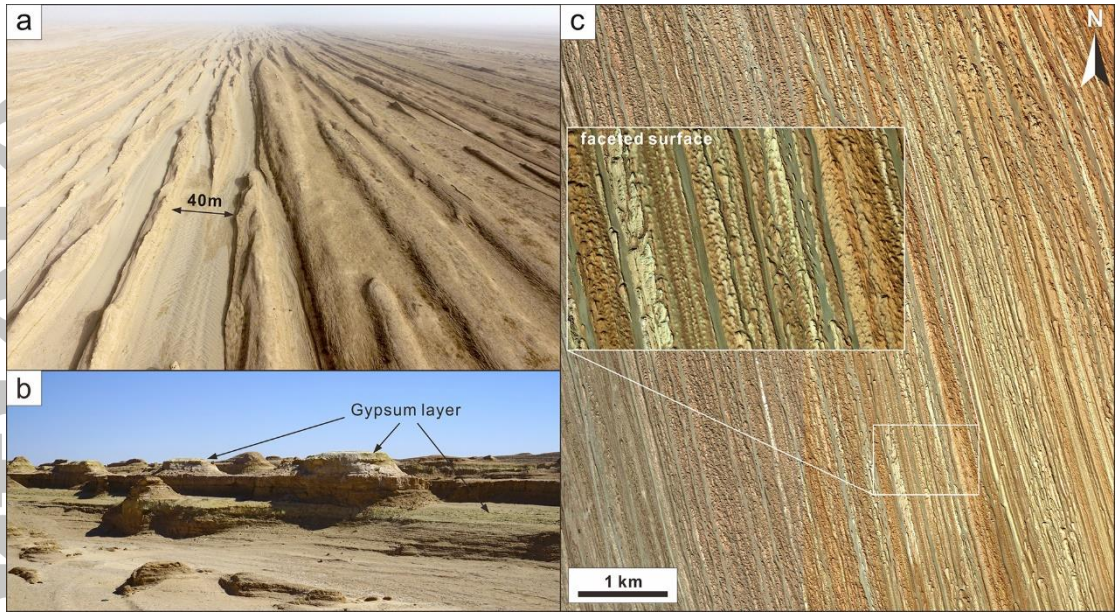

Figure 6. The narrow-top long-ridge (L-N type) and rough-top long-ridge (L-R type) yardangs in the Qaidam Basin. **(a)** The L-N type yardangs in southwest of Lenghu (38.52° N, 92.97° E). **(b)** Multilayered L-N type yardangs (38.66° N, 93.27° E). The greenish layer is enriched in gypsum. **(c)** L-R type yardangs in Lenghu (38.65° N, 92.78° E).

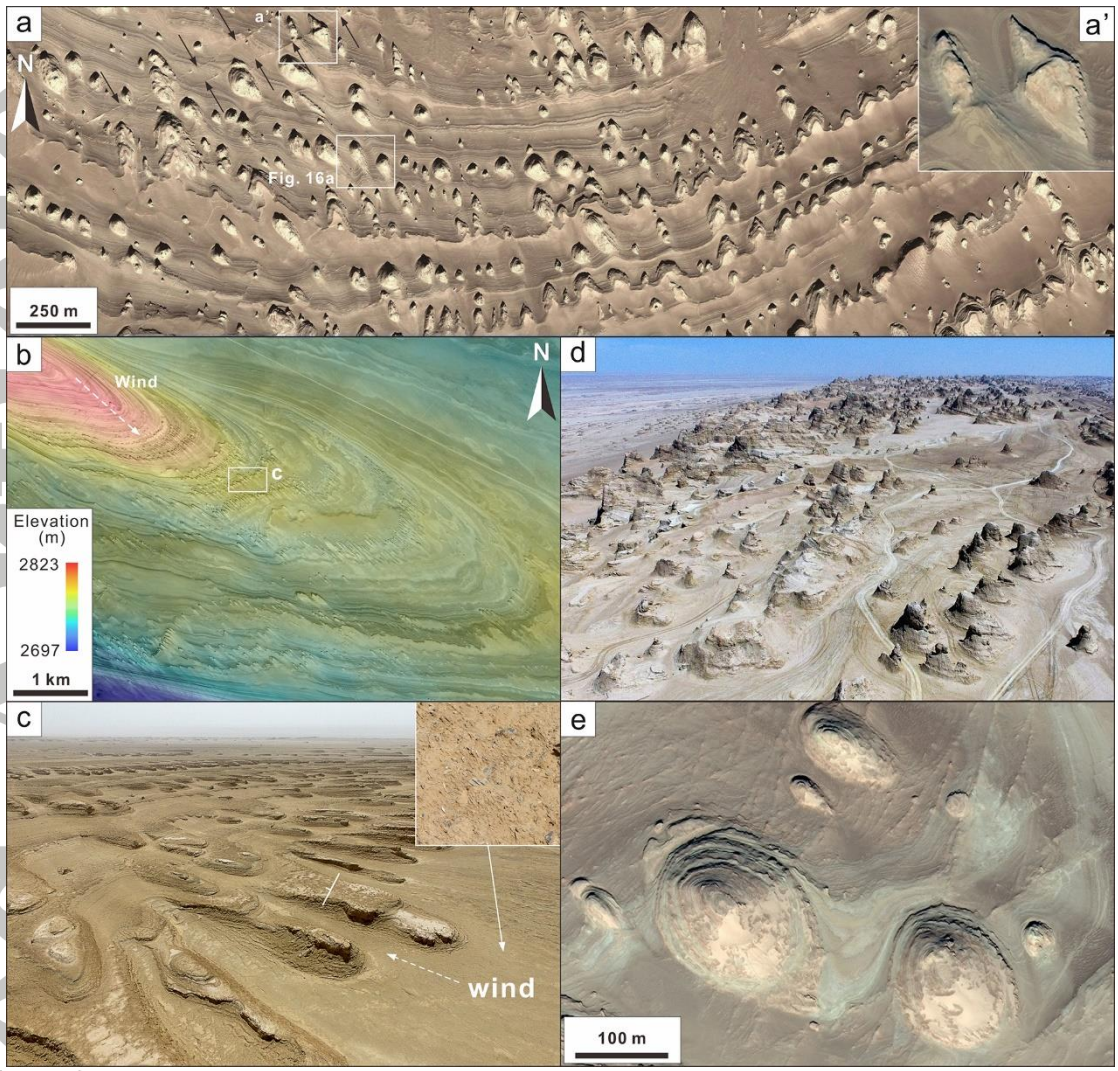

Figure 7. Saw-toothed group (S group) yardangs in the Qaidam Basin. **(a)** Group of the S-T type, S-P type and S-R type (remnant cone) yardangs (yellow arrows mark the fractures, image center: 37.62° N, 92.23° E). Inset a' shows that the yardangs are cut by fractures. **(b)** Google Terrain (SRTM-DEM) superposed on google images of the saw-toothed (S-T type) yardangs in the folded stratum (38.14° N, 91.87° E). **(c)** Perspective view using drone looking from north of the S-T type yardangs in (**b**), inset figure is the surface of the floor with gypsums. **(d)** The pyramid (S-P type) yardangs in the Daxiongshan uplift (E'boliang Yardang Geopark, image center: 38.35° N, 92.88° E). **(e)** The S-R type yardangs with rounded top and multiple layers (37.52° N, 92.30° E).

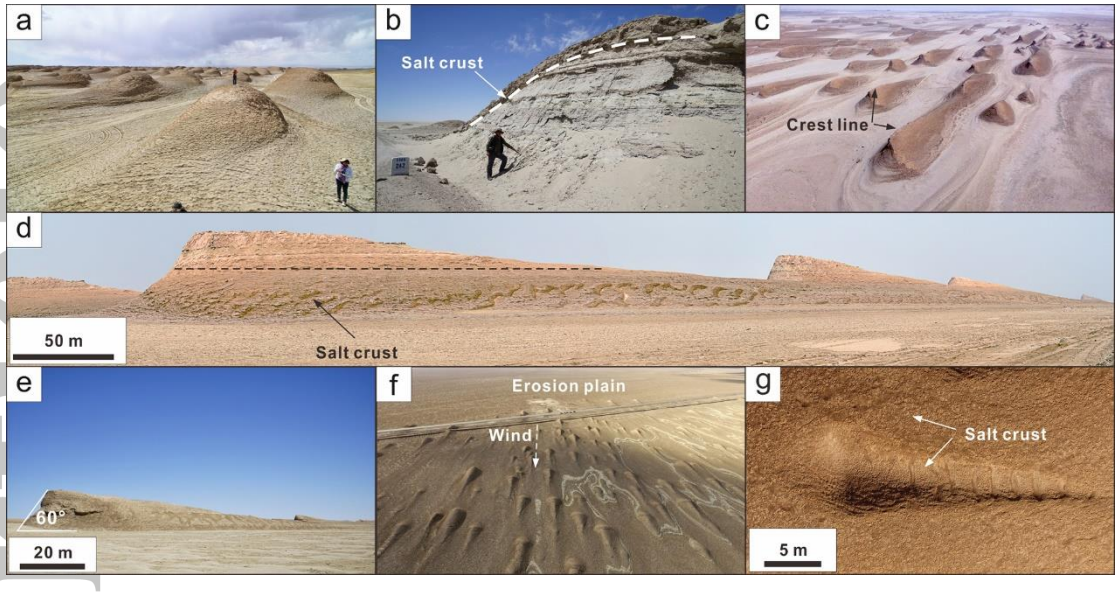

Figure 8. The whaleback group (W group) yardangs in the Qaidam Basin. **(a)** The whaleback (W-B type) yardangs in Nanyishan (38.41° N, 91.32° E). Their surfaces are covered by salt crusts. **(b)** A well-exposed profile of the W-B type yardang (38.24° N, 92.10° E). The salt crust on its top is 40-50cm thick. Bird's-eye view **(c)** and side-view **(d)** of large W-H type yardangs with sharp crestlines (38.38° N, 93.54° E). Their flanks are convex at the lower slopes but concave at their upper parts (black dashed line indicates the boundary in **(d)**. **(e)** A typical small hogback (W-H type) yardang with windward slope of ~60° (38.51° N, 92.91° E). **(f)** & **(g)** The low, streamlined whaleback (W-L type) yardangs in the north of East Taijinaier Lake (37.61° N, 94.18° E). The upwind area is an erosion plain. Salt crusts cover both of the surface of and the troughs of the yardangs.

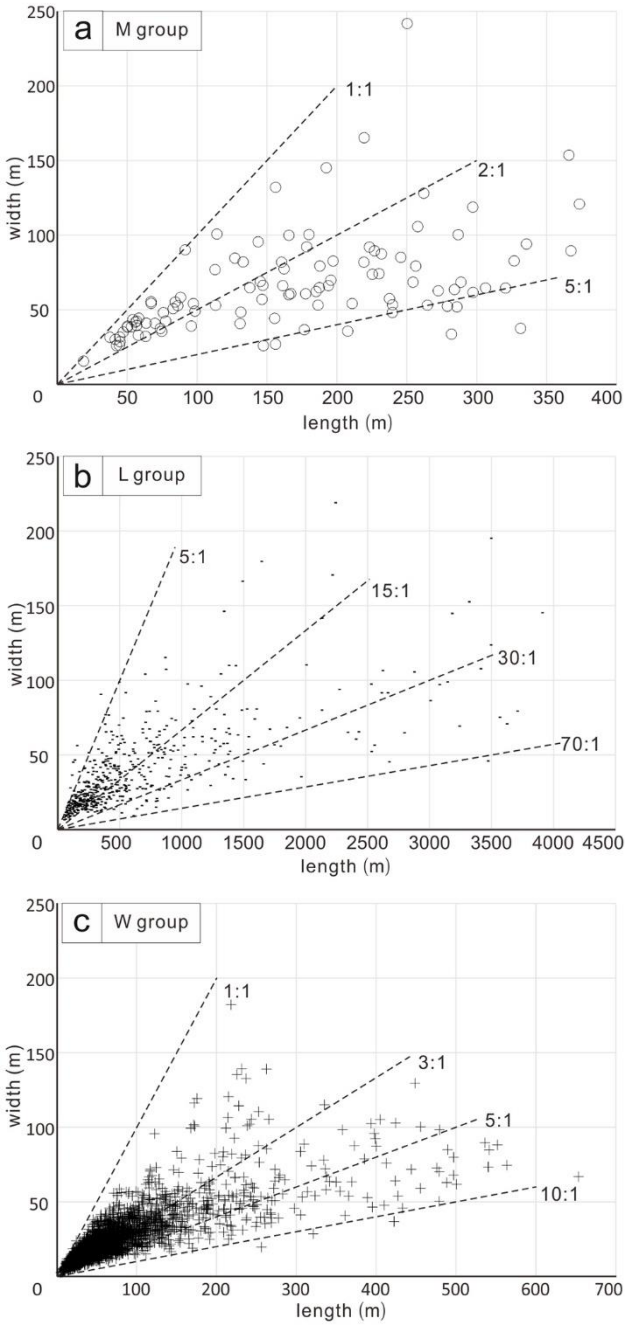

Figure 9. Aspect ratios of representative yardangs in the Qaidam Basin (data see Table S1 in Supplemental Material).

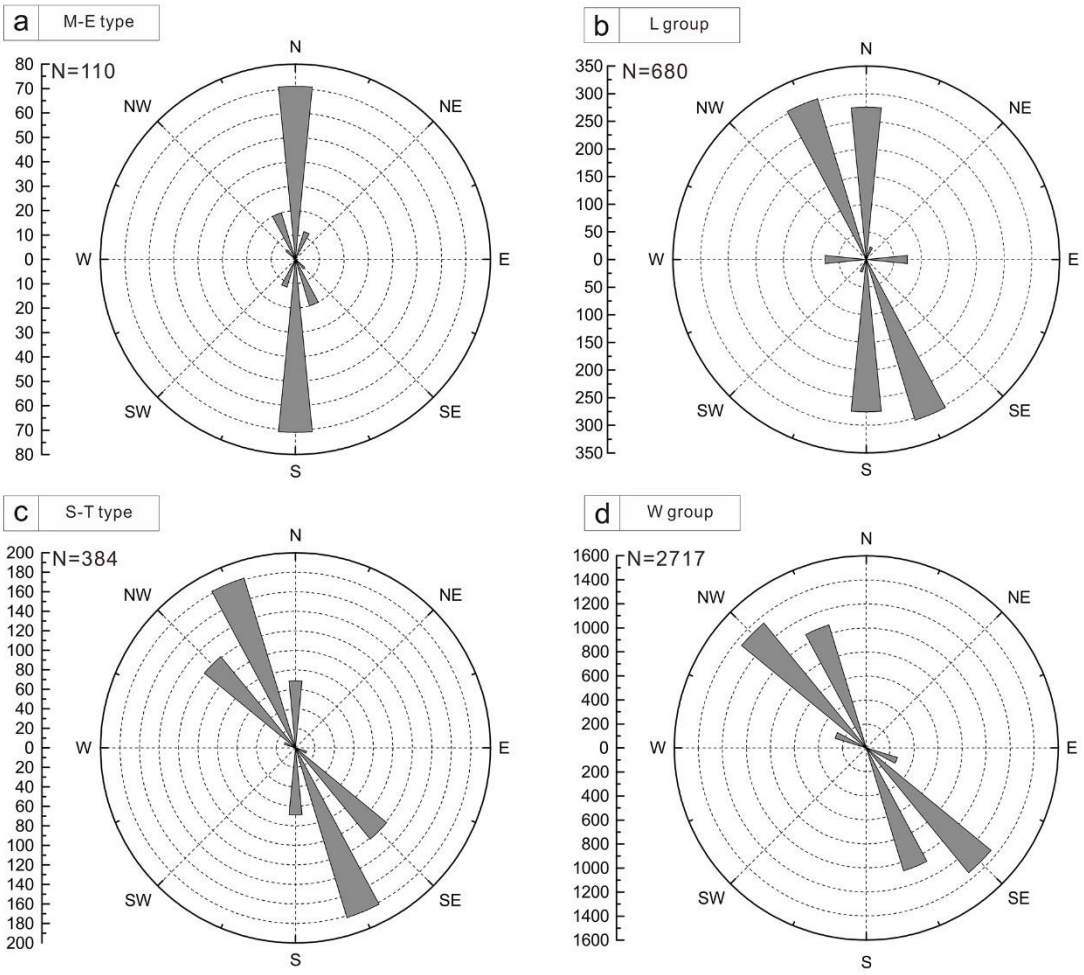

Figure 10. Orientations of typical yardang groups in the Qaidam Basin (data see Table S4 in Supplemental Material).

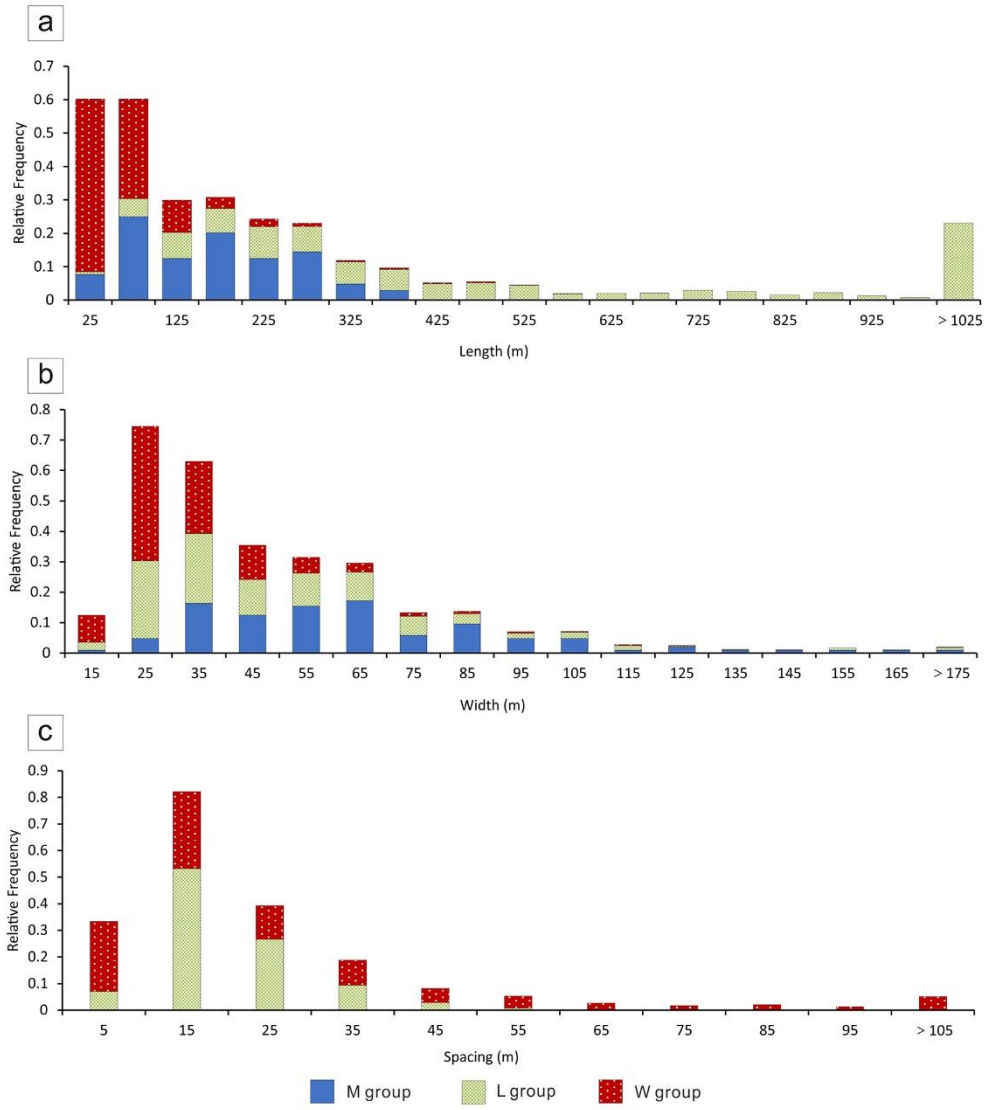

Figure 11. Relative frequency of length, width, and spacing of different yardang groups in the Qaidam Basin (data see Table S1 and S3 in Supplemental Material).

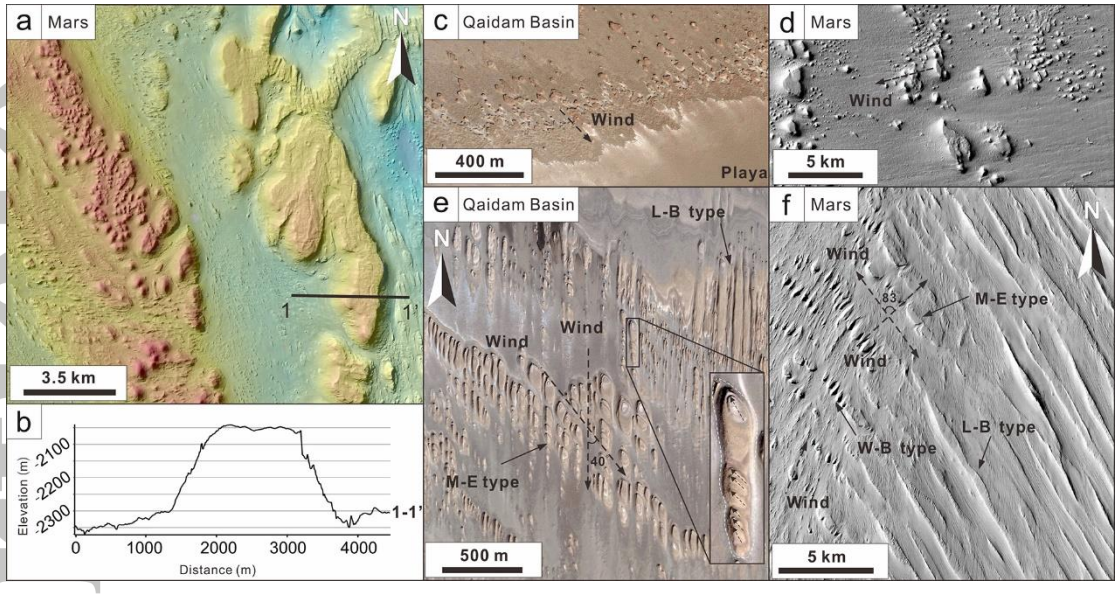

Figure 12. The evolution model for yardangs in the Qaidam Basin.

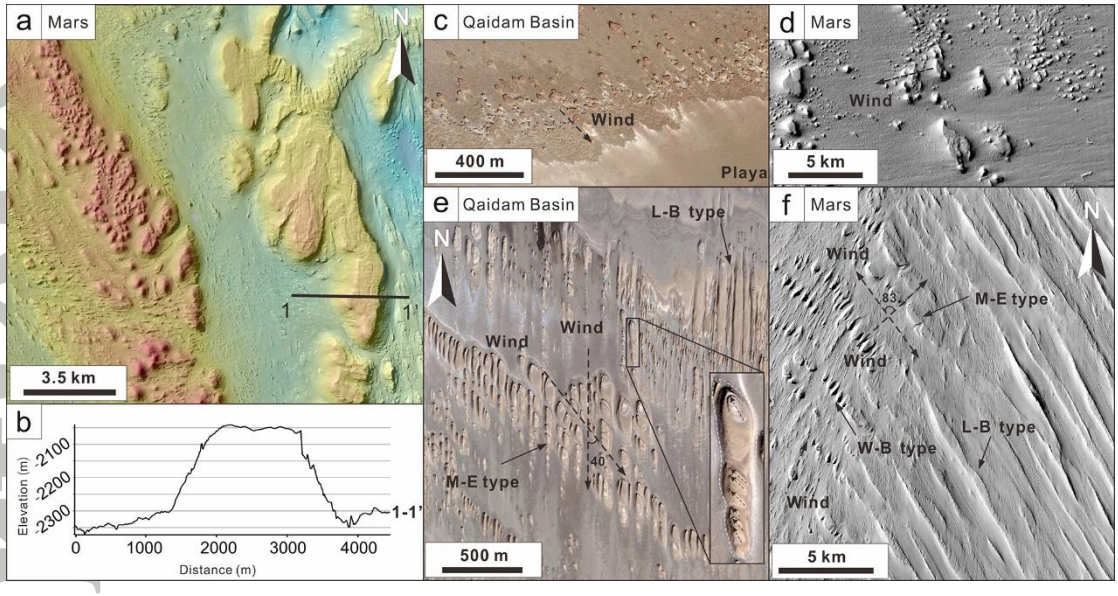

Figure 13. (a) The M-I type yardangs in Aeolis Dorsa of the Mars, CTX image with CTX DTM (f23_044686_1762_xi_03s209w/f19_043143_1761_xi_03s209w) overlay. Blue areas: lower elevations, red areas: higher elevations. (b) Elevation profile along 1-1' in figure a. (c) The M-I type yardangs at the western margin of playa (black arrows mark the wind directions, image center: 38.61° N, 91.30° E). (d) The M-I type yardangs in the continuous ejecta blanket of Mars (black arrows mark the wind directions, CTX image, p22_009821_1848_xi_04n211w). (e) The M-E type yardangs in the downwind direction of long-ridge group yardangs (black dashed arrows indicate two wind directions, image center: 38.00° N, 92.40° E), inset is the overlapped yardangs (white dashed line marks the outlines of the early stage yardangs, black dashed arrows mark the later stage yardangs). (f) The M-E type yardangs at Lucus Planum on Mars (black dashed line arrows indicate two wind directions. CTX image, p21_009200_1742_xi_05s176w).

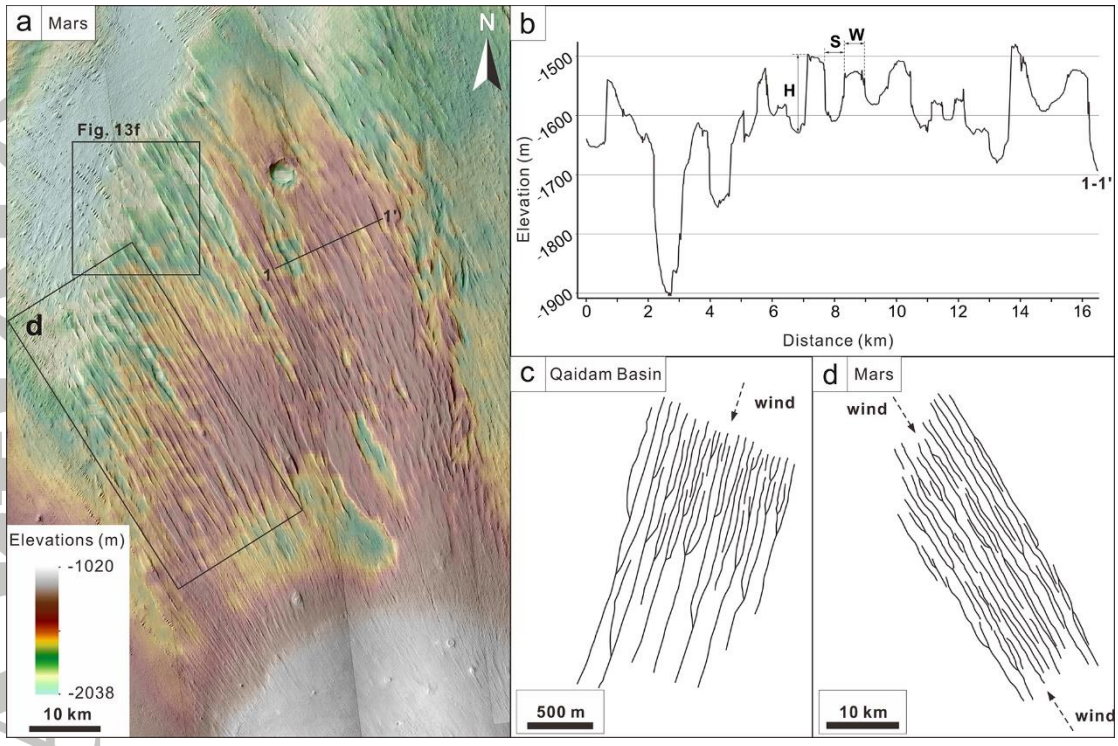

Figure 14. (a) The L-B type yardangs in the MFF area at Lucus Planum of Mars, CTX images (p21_009200_1742_xi_05s176w / p16_007262_1747_xn_05s176w) with a MOLA DTM overlay. (b) Elevation profile (CTX DTMs, p14_006550_1726_xn_07s175w / b17_016215_1728_xi_07s175w) along 1-1’ in figure a. (c) & (d) The schematic diagrams of the long axis of the L-B type yardangs in Figure 4a and Figure 12a.

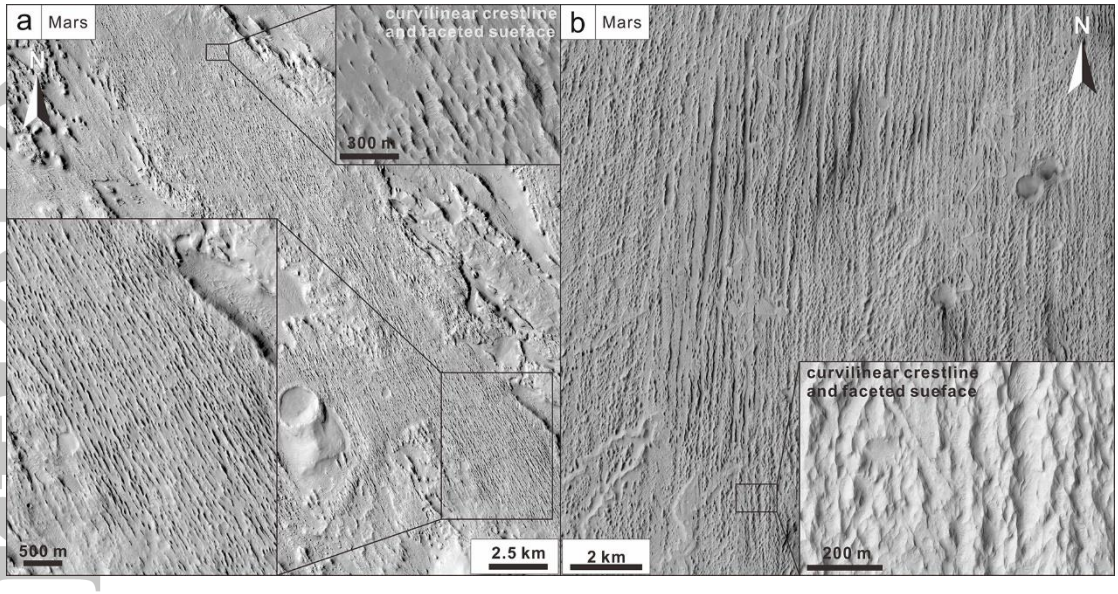

Figure 15. (a) The L-N type yardangs in Aeolis Serpens (CTX image, f03_036800_1762_xn_03s210w), inset figure of the upper right corner is part of HiRISE image (esp_036800_1750_red). **(b)** The L-R type yardangs in Aeolis Dorsa (CTX image, b16_016058_1739_xn_06s208w), inset figure of the bottom right corner is partial of HiRISE image (esp_016058_1740_red). The dark areas are sand sheets.

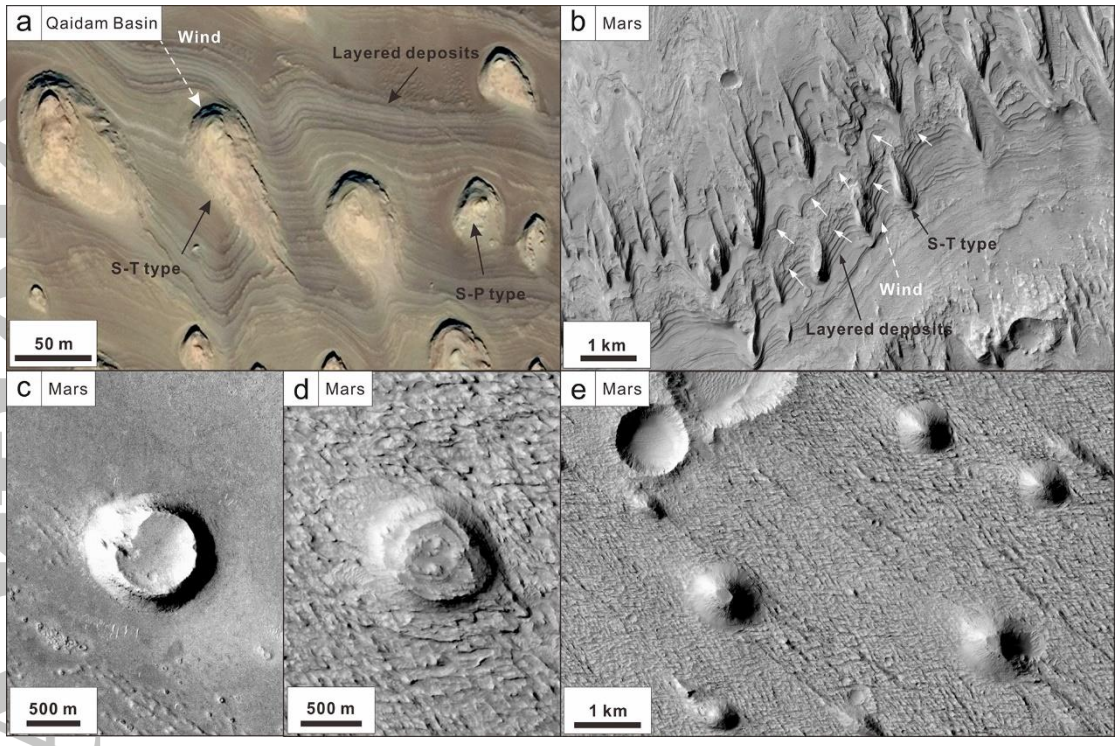

Figure 16. (a) The S-T and S-P type yardangs shown in Figure 7a in the Qaidam Basin. **(b)** The S-T type yardangs in Gale Crater (white dashed arrow indicates the wind directions, and white solid arrows mark the boundary between thin layer and anti-resistant layers. CTX image, f20_043750_1747_xn_05s221w). **(c), (d) & (e)** The S-R type yardangs formation processes that from degenerated crater floor to flat-top cone, then remnant cone yardangs, respectively (CTX images, **(c)** & **(d)** f07_038607_1821_xn_02n215w, **(e)** f02_036497_1830_xn_03n216w).

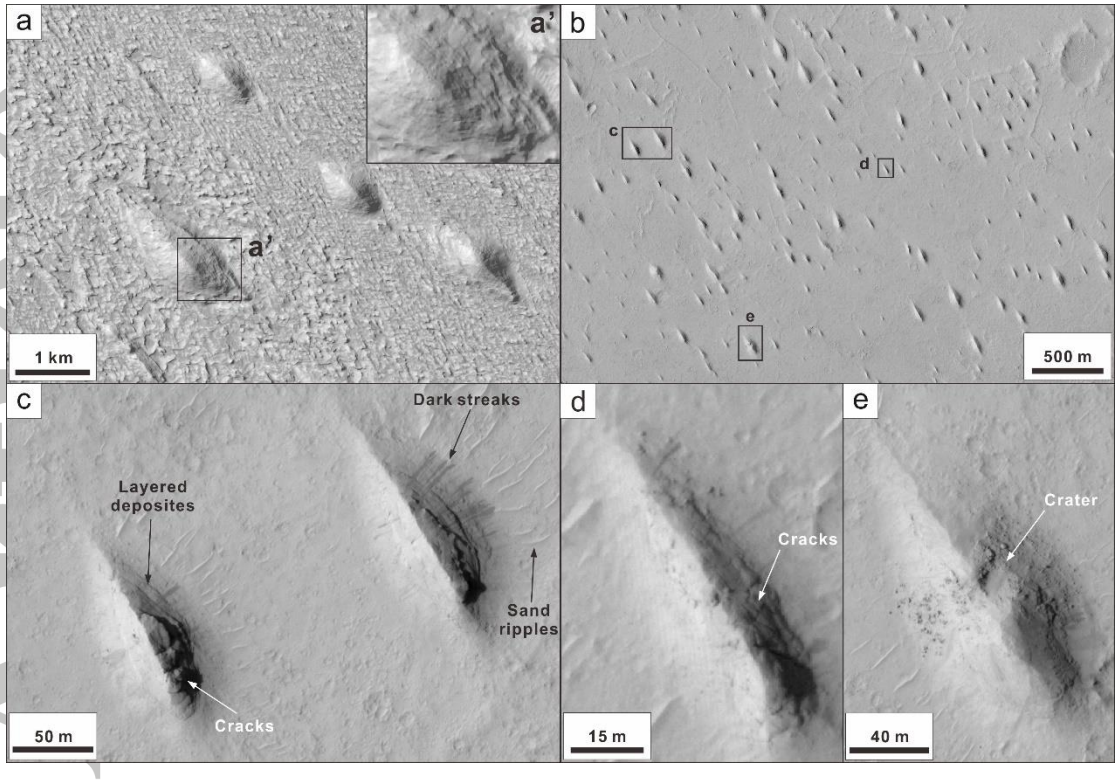

Figure 17. (a) The W-B type yardangs in Aeolis Planum on Mars (CTX image, d20_035231_1813_xn_01n215w). Inset a' shows the layered deposits. **(b)** The W-H type yardangs in Zephyria Planum (HiRISE image, psp_066828_1820_red). **(c) & (d)** Large and small size W-H type yardangs shown in (**b**). **(e)** The W-H type yardang was partially destroyed by impact crater.

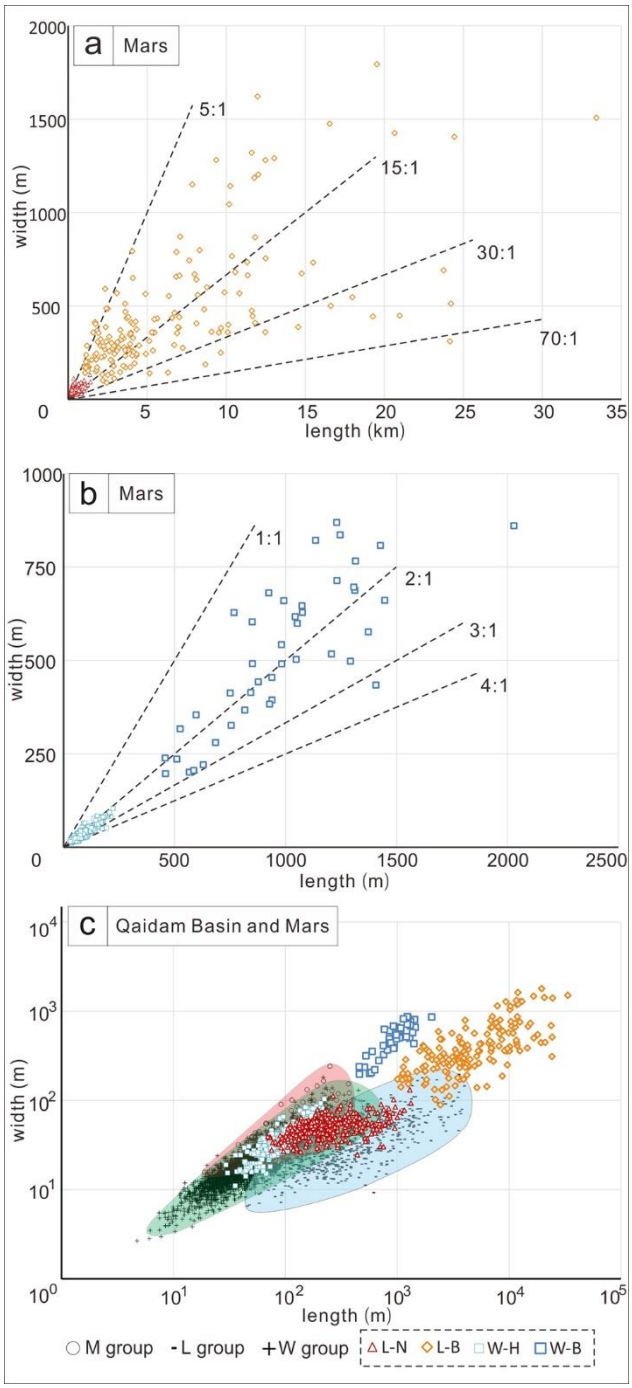

Figure 18. Aspect ratios of representative yardangs in MFF and Gale Crater on Mars and their comparison with the Qaidam Basin on Earth. **(a)** The L-B and L-N type yardangs. **(b)** The W-B and W-H type yardangs. **(c)** Log-log plot of lengths versus widths of these seven different yardangs both in the Qaidam Basin on Earth and in MFF and Gale Crater on Mars. Red, green, and blue areas are the M, L, and W group yardangs in the Qaidam Basin, respectively.

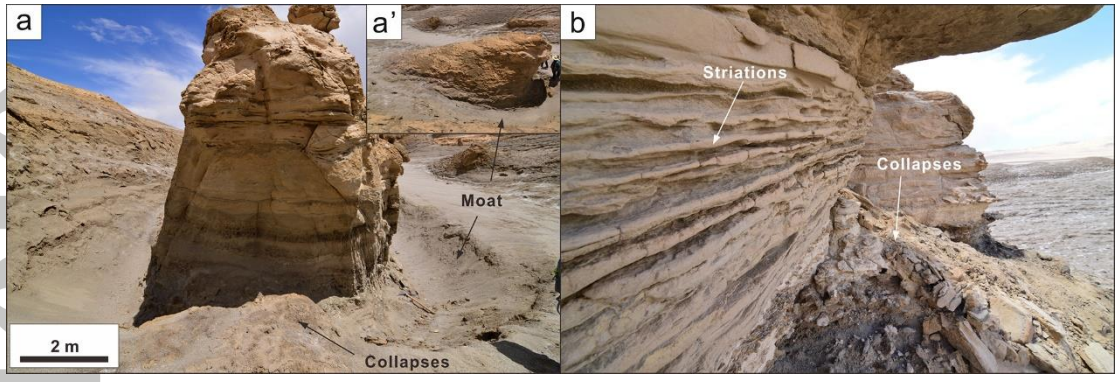

Figure 19. (a) Moat on the upwind face and flanks (38.49° N, 91.16° E). Collapsed material occurs in the upwind direction. **(b)** Striations on the flank (38.50° N, 91.16° E).

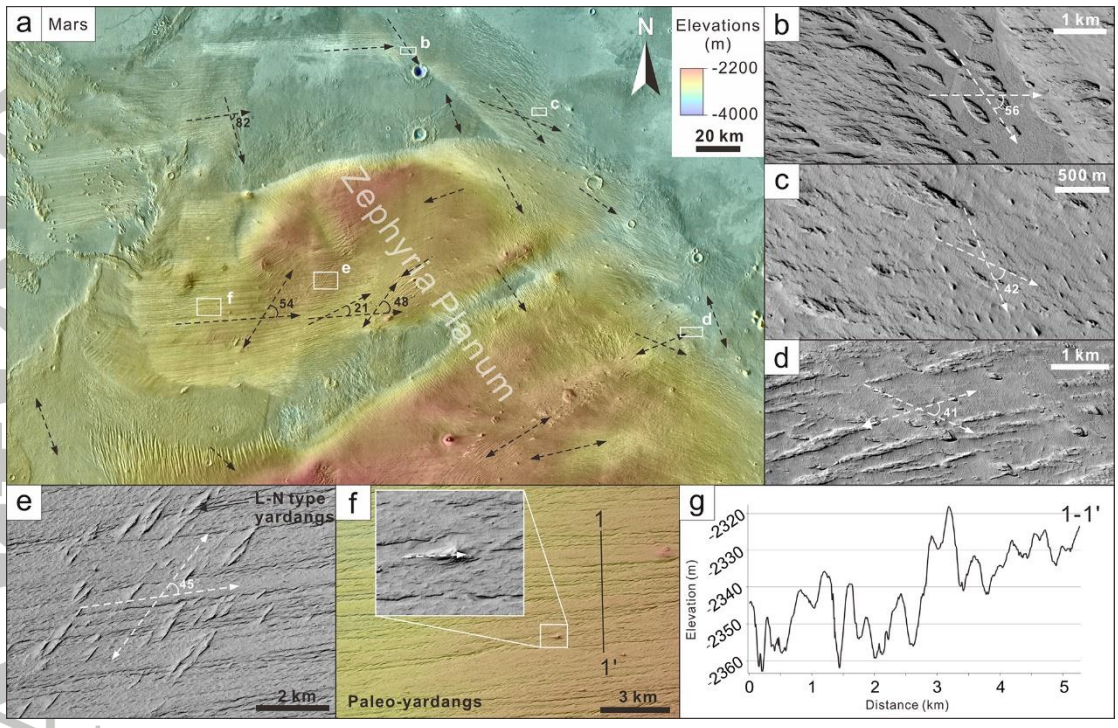

Figure 20. (a) Yardangs and paleo-yardangs in the North Zephyria Planum, THEMIS Day IR image (Edwards et al., 2011) superposed on HRSC DTMs (h2110_0000_dt4, h2121_0000_dt4, h2143_0000_dt4, h2154_0000_dt4, h2165_0001_dt4, h2176_0000_dt4), black dashed lines mark the orientation of yardangs. **(b)**, **(c)**, & **(d)** The variation of yardang orientations at the eastern area in (**a**) (white dashed lines mark the orientations of yardangs, CTX images, b09_013302_1844_xn_04n208w, b06_011957_1865_xn_05n207w, f23_044844_1818_xn_01n205w). **(e)** & **(f)** L-B type paleo-yardangs shown in (**a**). **(g)** Elevation profile along 1-1' in figure f.

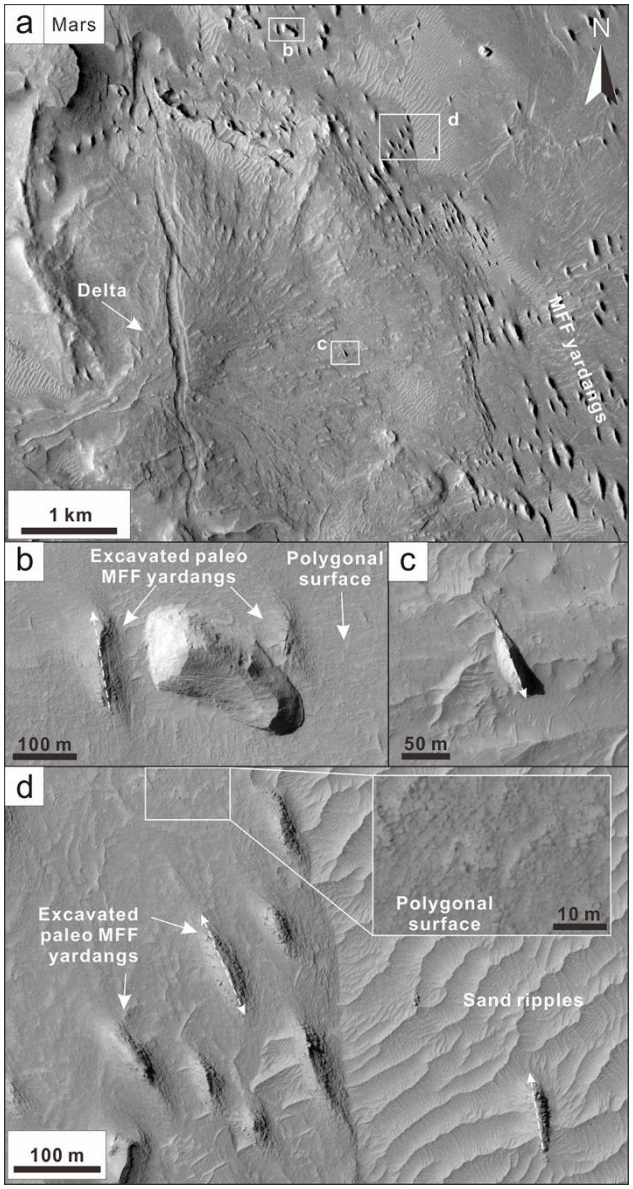

Figure 21. (a) Delta and yardangs in the Gunjur crater (CTX image, d15_033108_1798_xn_00s213w). **(b)** The excavated paleo MFF yardangs (white dashed line marks the orientation of yardang, HiRISE image, psp_007883_1800_red). **(c)** The remnant yardang on the surface of delta deposits (white dashed line marks the orientation of yardang, HiRISE image, psp_007883_1800_red). **(d)** The excavated yardangs (white dashed line marks the orientation of yardang, HiRISE image, psp_007883_1800_red). Polygonal features are obvious on the floor layer.

Table 1. Classification of the yardangs in the Qaidam Basin. Modified after Halimov & Fezer (1989) and Li et al. (2016).

Type	Characteristic	Group
Irregular mesa (M-I type)	Flat top, irregular in shape, cliffs, ambiguous orientations	Mesa （M group）
Elongated mesa (M-E type)	Flat top at the head, arranged to lines in one direction or two directions	
Broad-top long-ridge (L-B type)	Broad top, narrow troughs, gentle slope flanks, salt crust	Long-ridge （L group）
Narrow-top long-ridge (L-N type)	Narrow top, broad troughs, steep flanks	
Rough-top long-ridge (L-R type)	Broken top, ambiguous morphology	
Saw-toothed (S-T type)	Upwind zigzag-like shape, downwind areas are mostly unaltered	Saw-toothed (S group)
Pyramid (S-P type)	Large base with spire top	
Remnant cone (S-R type)	Large base with rounded shape or small flat area on its top	
Whaleback (W-B type)	Classic form with blunt head and tapered tail, salt crust on the surface	Whaleback (W group)
Hogback (W-H type)	Steep windward heads (＞60 °) with sharp crests on their backs, and some have undercut windward heads	
Low, streamlined whaleback (W-L type)	Low height, streamlined morphology, large spacing	

Table 2. Statistical summary of measured morphological parameters for different yardang groups (see Figure S1, Table S1, S2, and S3 in Supplemental Material).

		M group	L group	W group
Length (m)	Range	18–374	43–3903	5–654
	Mean	167	634	71
	Median	162	389	48
	S.D.	92	687	69
	C.V.	0.55	1.08	0.98
Width (m)	Range	15–242	6–219	3–182
	Mean	66	39	24
	Median	59	30	19
	S.D.	34	29	17
	C.V.	0.51	0.74	0.69
Aspect ratio	Range	1:1–8.8:1	2.6–75.4:1	1.1:1–13:1
	Mean	2.7:1	15.5:1	2.8:1
	Median	2.3:1	12.5:1	2.5:1
	S.D.	1.51:1	10.03:1	1.18:1
	C.V.	0.56	0.65	0.42
Spacing (m)	Range	–	4–76	2–339
	Mean	–	20	31
	Median	–	17.8	18
	S.D.	–	9.08	36
	C.V.	–	0.45	1.17
Height (m)	Range	Up to ~20	Up to ~30	0.5–30

–: not measured. S.D. - Standard Deviation; C.V. - Coefficient of Variation. The M-I type yardangs are not included in the M group. The heights of yardangs are estimated from a few measurements in the field.

Table 3. Comparison of yardangs in the Qaidam Basin and their analogues in MFF and Gale Crater on Mars.

Group	Type	Qaidam Basin, MFF and Gale Crater	Qaidam Basin	MFF and Gale Crater
		Similarity	Difference	
M group	M-I	Dendritic shape; Coexisting with the W group yardangs	The W group yardangs developed only in the erosion floors.	The W group yardangs developed both on the surface and the erosion depressions.
	M-E	Coexisting with L-B type or W group yardangs; Protecting layers on the surface.	Gravel-enriched. polygonal surface layer	An indurated (some degree) surface layer.
L group	L-B	Large scale in fields; Coexisting with L-N type yardangs.	Straight crestline; Salt crust surface layer; "Cap layer" on top.	Curvilinear crestline; Double tined heads; Faceted surface with interwoven wind streaks.
	L-N	Coexisting with W group yardangs.	"Cap layer" on top.	Curvilinear crestlines.
	L-R	Faceted surface.	Unidirectional features	Bidirectional features on the surface.
S group	S-T	Developed in fine layers.	–	–
W group	W-B	Streamlined shape.	Covered by salt crust.	Rare on mars; Developed in fined-layers; Large in size.
	W-H	Sand ripples surrounded.	Lower parts are usually covered by salt crusts.	Some of them with double tapered heads; Blocky surface with dusts covered.

–: none.